Guide to C-Mod GPI camera data

S.J. Zweben and J.L. Terry
v. 4
1/17/18

OUTLINE

1. GPI hardware history (Jim to correct as needed)

2001 - photodiode array, Xybion
2002 - Princeton Scientific Instruments PSI-3
2004 - Princeton Scientific Instruments PSI-5
2005 - 1D APD array
2007 - Phantom 7.3 (two used at C-Mod)
2007 - X-region view installed
2009 - two quartz coherent bundles replace Schott glass bundles
2009 - Phantom 710 (two used at C-Mod)
2010 - 2D APD array at outer midplane

present location of C-Mod GPI hardware:

Phantom 710s – brought back to PPPL, one given to Brent Stratton for NSTX GPI, the other given to Raffi Nazikian for DIII-D
Phantom 7.3s – one loaned to Filippo Scotti for NSTX (owned by Brent), one given to Doug Darrow for NSTX (?)
quartz fiberoptic bundles – presently in Stewart's office (not on property list)
GPI telescopes – left inside C-Mod vessel
GPI camera mounts and optical benches – left on top of C-Mod

2. Active collaborators

Brian LaBombard and Jerry Hughes – MIT
Matteo Agostini and Paolo Scarin – RFX group Padova
Olaf Grulke – IPP Greifswald, Germany
Daren Stotler - PPPL
Ralph Kube and O.E. Garcia – Tromso, Norway
Istvan Cziegler and J. Sierchio - MIT
Bruce Scott and Klaus Hallatschek - Garching, Germany
Federico Halpern and Paolo Ricci - Lausanne, Switzerland
Jim Myra, Dan D'Ippolito and David Russell – Lodestar
Maxim Umansky and Ron Cohen - LLNL

3. Publications

GPI camera diagnostic results (selected from WOS "Terry + Zweben")

Invited Review Article: Gas puff imaging diagnostics of edge plasma turbulence in magnetic fusion devices
By: Zweben, S. J.; Terry, J. L.; Stotler, D. P.; et al.
REVIEW OF SCIENTIFIC INSTRUMENTS Volume: 88 Issue: 4 Article Number: 041101 Published: APR 2017

Comparison of velocimetry techniques for turbulent structures in gas-puff imaging data
By: Sierchio, J. M.; Cziegler, I.; Terry, J. L.; et al.
Conference: 16th International Conference on Ion Sources (ICIS) Location: New York, NY Date: AUG 23-28, 2015
Sponsor(s): Brookhaven Natl Lab, Collider Accelerator Dept
REVIEW OF SCIENTIFIC INSTRUMENTS Volume: 87 Issue: 2 Article Number: 023502 Published: FEB 2016

Blob sizes and velocities in the Alcator C-Mod scrape-off layer
By: Kube, R.; Garcia, O. E.; LaBombard, B.; et al.
Conference: 20th International Conference on Plasma-Surface Interactions in Controlled Fusion Devices (PSI) Location: Forschungszentrum Julich, Aachen, GERMANY Date: MAY 21-25, 2012
JOURNAL OF NUCLEAR MATERIALS Volume: 438 Supplement: S Pages: S505-S508 Published: JUL 2013

Comparison of edge turbulence imaging at two different poloidal locations in the scrape-off layer of Alcator C-Mod
By: Zweben, S. J.; Terry, J. L.; Agostini, M.; et al.
PHYSICS OF PLASMAS Volume: 20 Issue: 7 Article Number: 072503 Published: JUL 2013

Search for zonal flows in the edge turbulence of Alcator C-Mod
By: Zweben, S. J.; Terry, J. L.; Agostini, M.; et al.
Group Author(s): Alcator C-Mod Grp

PLASMA PHYSICS AND CONTROLLED FUSION Volume: 54 Issue: 2 Article Number: 025008 Published: FEB 2012

Estimate of convective radial transport due to SOL turbulence as measured by GPI in Alcator C-Mod
By: Zweben, S. J.; Terry, J. L.; LaBombard, B.; et al.
Conference: 19th International Conference on Plasma-Surface Interactions in Controlled Fusion Devices (PSI) Location: Univ Calif, Gen Atom, San Diego, CA Date: MAY 24-28, 2010
Sponsor(s): Lawrence Livermore Natl Lab
JOURNAL OF NUCLEAR MATERIALS Volume: 415 Issue: 1 Supplement: S Pages: S463-S466 Published: AUG 1 2011

Edge turbulence in different density regimes in Alcator C-Mod experiment
By: Agostini, M.; Terry, J. L.; Scarin, P.; et al.
NUCLEAR FUSION Volume: 51 Issue: 5 Article Number: 053020 Published: MAY 2011

On the statistics of edge fluctuations: comparative study between various fusion devices
By: Sattin, F.; Agostini, M.; Scarin, P.; et al.
PLASMA PHYSICS AND CONTROLLED FUSION Volume: 51 Issue: 5 Article Number: 055013 Published: MAY 2009

Spatial structure of scrape-off-layer filaments near the midplane and X-point regions of Alcator-C-Mod
By: Terry, J. L.; Zweben, S. J.; Umansky, M. V.; et al.
Conference: 18th International Conference on Plasma-Surface Interactions in Controlled Fusion Devices Location: Toledo, SPAIN Date: MAY 26-30, 2008
Sponsor(s): Spanish Natl Fus Lab; Spanish Minist Sci & Innovat
JOURNAL OF NUCLEAR MATERIALS Volume: 390-91 Pages: 339-342 Published: JUN 15 2009

Structure and motion of edge turbulence in the national spherical torus experiment and alcator C-mod
By: Zweben, S. J.; Maqueda, R. J.; Terry, J. L.; et al.
Conference: 47th Annual Meeting of the Division of Plasma Physics of the American-Physical-Society Location: Denver, CO Date: OCT 24-28, 2005
Sponsor(s): Amer Phys Soc, Div Plasma Phys
PHYSICS OF PLASMAS Volume: 13 Issue: 5 Article Number: 056114 Published: MAY 2006

Radially propagating fluctuation structures in the scrape-off layer of Alcator C-Mod
By: Grulke, O; Terry, JL; LaBombard, B; et al.
PHYSICS OF PLASMAS Volume: 13 Issue: 1 Article Number: 012306 Published: JAN 2006

Transport phenomena in the edge of Alcator C-Mod plasmas
By: Terry, JL; Basse, NP; Cziegler, I; et al.
NUCLEAR FUSION Volume: 45 Issue: 11 Pages: 1321-1327 Published: NOV 2005

Velocity fields of edge/Scrape-off-layer turbulence in Alcator C-Mod
By: Terry, JL; Zweben, SJ; Grulke, O; et al.

Conference: 16th International Conference on Plasma Surface Interactions in Controlled Fusion Devices Location: Portland, ME Date: MAY 24-28, 2004
Sponsor(s): MIT, Plasma Sci & Fus Ctr; US DOE
JOURNAL OF NUCLEAR MATERIALS Volume: 337 Issue: 1-3 Pages: 322-326 Published: MAR 1 2005

High speed movies of turbulence in Alcator C-Mod
By: Terry, JL; Zweben, SJ; Bose, B; et al.
Conference: 15th Topical Conference on High-Temperature Plasma Diagnostics Location: San Diego, CA Date: APR 19-22, 2004
Sponsor(s): Amer Phys Soc; US DOE; Gen Atom
REVIEW OF SCIENTIFIC INSTRUMENTS Volume: 75 Issue: 10 Pages: 4196-4199 Part: 2 Published: OCT 2004

Observations of the turbulence in the scrape-off-layer of Alcator C-Mod and comparisons with simulation
By: Terry, JL; Zweben, SJ; Hallatschek, K; et al.
Conference: 44th Annual Meeting of the Division of Plasma Physics of the American-Physical-Society Location: ORLANDO, FL Date: NOV 11-15, 2002
Sponsor(s): Amer Phys Soc, Div Plasma Phys
PHYSICS OF PLASMAS Volume: 10 Issue: 5 Pages: 1739-1747 Part: 2 Published: MAY 2003

Gas puff imaging of edge turbulence (invited)
By: Maqueda, RJ; Wurden, GA; Stotler, DP; et al.
Conference: 14th Topical Conference on High-Temperature Plasma Diagnostics Location: MADISON, WISCONSINDate: JUL 08-11, 2002
Sponsor(s): Univ Wisconsin Madison; Amer Phys Soc, Div Plasma Phys; US DOE, Off Fus Energy Sci & Defense Sci
REVIEW OF SCIENTIFIC INSTRUMENTS Volume: 74 Issue: 3 Special Issue: SI Pages: 2020-2026 Part: 2 Published: MAR 2003

Edge turbulence imaging in the Alcator C-Mod tokamak
By: Zweben, SJ; Stotler, DP; Terry, JL; et al.
Group Author(s): Alcator C-Mod Grp
Conference: 43rd Annual Meeting of the Division of Plasma Physics of the American-Physical-Society Location: LONG BEACH, CALIFORNIA Date: OCT 29-NOV 02, 2001
Sponsor(s): Amer Phys Soc, Div Plasma Phys
PHYSICS OF PLASMAS Volume: 9 Issue: 5 Pages: 1981-1989 Part: 2 Published: MAY 2002

Visible imaging of turbulence in the SOL of the Alcator C-Mod tokamak
By: Terry, JL; Maqueda, R; Pitcher, CS; et al.
Conference: 14th International Conference on Plasma-Surface Interactions in Conrtrolled Fusion Devices Location: ROSENHEIM, GERMANY Date: MAY 22-26, 2000
JOURNAL OF NUCLEAR MATERIALS Volume: 290 Pages: 757-762 Published: MAR 2001

Comparisons of GPI results with theory (selected from WOS "Terry + Zweben"):

Outer midplane scrape-off layer profiles and turbulence in simulations of Alcator C-Mod inner-wall limited discharges
By: Halpern, Federico D.; LaBombard, Brian; Terry, James L.; et al.
PHYSICS OF PLASMAS Volume: 24 Issue: 7 Article Number: 072502 Published: JUL 2017

Mean flows and blob velocities in scrape-off layer (SOLT) simulations of an L-mode discharge on Alcator C-Mod
By: Russell, D. A.; Myra, J. R.; D'Ippolito, D. A.; et al.
PHYSICS OF PLASMAS Volume: 23 Issue: 6 Article Number: 062305 Published: JUN 2016

Comparison of 3D flux-driven scrape-off layer turbulence simulations with gas-puff imaging of Alcator C-Mod inner-wall limited discharges
By: Halpern, F. D.; Terry, J. L.; Zweben, S. J.; et al.
Conference: Joint Varenna-Lausanne International Workshop on the Theory of Fusion Plasmas Location: Varenna, ITALY Date: SEP 01-05, 2014
PLASMA PHYSICS AND CONTROLLED FUSION Volume: 57 Issue: 5 Article Number: 054005 Published: MAY 2015

Overview of experimental results and code validation activities at Alcator C-Mod
By: Greenwald, M.; Bader, A.; Baek, S.; et al.
NUCLEAR FUSION Volume: 53 Issue: 10 Special Issue: SI Article Number: 104004 Published: OCT 2013

Edge sheared flows and the dynamics of blob-filaments
By: Myra, J. R.; Davis, W. M.; D'Ippolito, D. A.; et al.
NUCLEAR FUSION Volume: 53 Issue: 7 Article Number: 073013 Published: JUL 2013

Numerical investigation of edge plasma phenomena in an enhanced D-alpha discharge at Alcator C-Mod: Parallel heat flux and quasi-coherent edge oscillations
By: Russell, D. A.; D'Ippolito, D. A.; Myra, J. R.; et al.
PHYSICS OF PLASMAS Volume: 19 Issue: 8 Article Number: 082311 Published: AUG 2012

Comparison of scrape-off layer turbulence in Alcator C-Mod with three dimensional gyrofluid computations
By: Zweben, S. J.; Scott, B. D.; Terry, J. L.; et al.
PHYSICS OF PLASMAS Volume: 16 Issue: 8 Article Number: 082505 Published: AUG 2009

Theory and fluid simulations of boundary-plasma fluctuations
By: Cohen, R. H.; LaBombard, B.; Ryutov, D. D.; et al.
NUCLEAR FUSION Volume: 47 Issue: 7 Pages: 612-625 Published: JUL 2007

Observations of the turbulence in the scrape-off-layer of Alcator C-Mod and comparisons with simulation
By: Terry, JL; Zweben, SJ; Hallatschek, K; et al.

Conference: 44th Annual Meeting of the Division of Plasma Physics of the American-Physical-Society Location: ORLANDO, FL Date: NOV 11-15, 2002
Sponsor(s): Amer Phys Soc, Div Plasma Phys
PHYSICS OF PLASMAS Volume: 10 Issue: 5 Pages: 1739-1747 Part: 2 Published: MAY 2003

Neutral transport simulations of gas puff imaging experiments
By: Stotler, DP; LaBombard, B; Terry, JL; et al.
Conference: 15th International Conference on Plasma-Surface Interactions in Controlled Fusion Devices (PSI-15)Location: GIFU, JAPAN Date: MAY 26-31, 2002
JOURNAL OF NUCLEAR MATERIALS Volume: 313 Pages: 1066-1070 Article Number: PII S0022-3115(02)01495-2 Published: MAR 2003

Ten most highly cited of these papers (as of 1/18)

Zweben PPCF 2002 – 175
Terry PoP 2003 – 162
Grulke PoP 2006 – 78
Maqueda RSI 2003 – 77
Terry JNM 2001 – 59
Zweben PoP '06 – 56
Terry NF 2005 – 51
Stotler HNM 2003 – 39
Zweben PoP 2009 – 35
Terry JNM 2005 - 34

4. Overview of GPI data

A schematic view of the GPI camera system on C-Mod is shown in Fig. 4.1, taken from the GPI review paper Zweben, Terry et al, RSI 2017. After 2009 there were two Phantom 710 cameras, one viewing the separatrix region near the outer midplane and one viewing the X-point region below. Each had its own GPI gas nozzle and computer-controlled data acquisition, and these could be operated singly or together. Most of this Guide will focus on the outer midplane camera, and the X-region system will be discussed in Sec. 9.

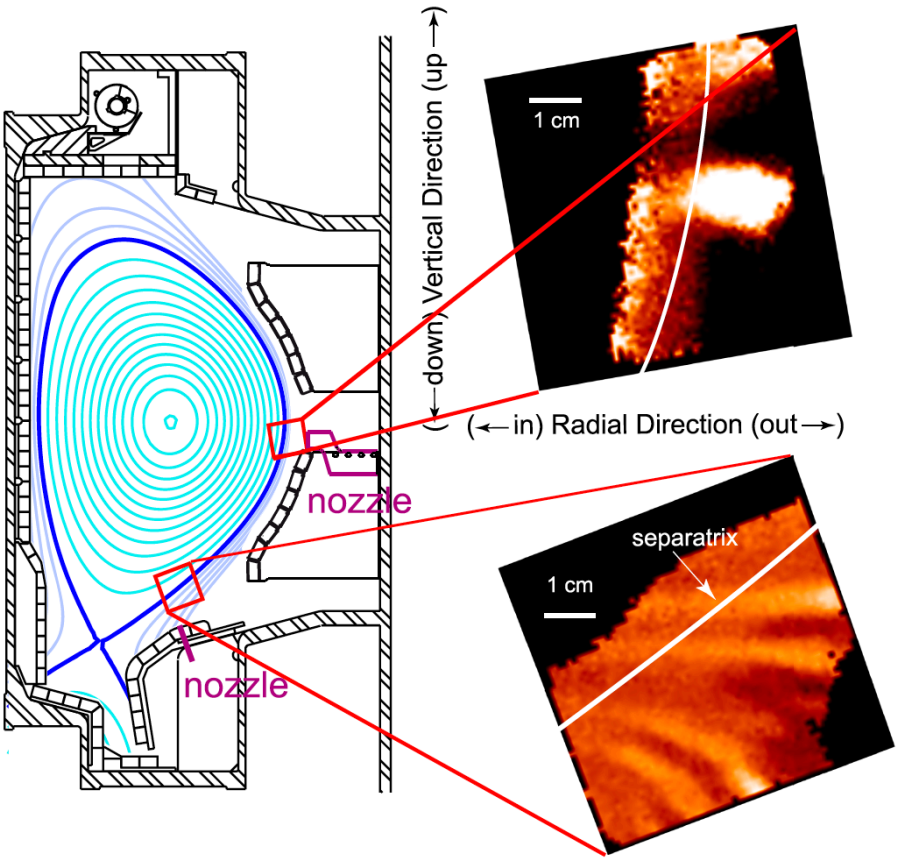

Fig. 4.1 GPI camera views in C-Mod

4.1 How GPI cameras were used

The GPI cameras on C-Mod were not operated automatically on every shot, but had to be started and operated specifically for each run day. This was normally done by Jim or sometimes by Stewart when he was visiting (at most one week a month). The setup involved turning on the GPI camera computer in the control room, making sure that the desired filter was installed in front of the camera lens on top of the machine (Dalpha 662 nm or HeI 587.6 nm), defining the camera settings, and preparing the appropriate gas puff through the Ninja system.

Once started in the morning, the camera acquisition would continue until stopped at the end of the run day. The same process was used for both the outer midplane and X-point region cameras. Sometimes both were operated on the same day. The GPI operator each day had the choice of camera filter and GPI gas, camera framing rate, camera start time, camera pixel format, and number of frames to capture. Typically these were 400,000 frames/sec with 64x64 pixels for 30,000 frames for the Phantom 710s since 2009, at least for those runs looking at turbulence.

There were no optical hardware adjustments done on the GPI between machine openings, except for filter changes. The telescopes were inside the machine and the cameras were fixed to their optical benches on top of the machine. Usually the optics was checked and cleaned each machine opening by Jim, including alignment with a target inside the vessel. After the quartz bundles were installed in 2009, no changes in the optics were done, as far as I (sz) know. Earlier Schott glass bundles were replaced once or twice for browning. The telescope alignments might have been tweaked once or twice, but their mounting location on the inside vessel walls were never changed (Jim should comment on this). The camera alignment or 'registration' information was stored on the MDS+ tree, as described in Sec. 5.

4.2 Best camera data for future analysis (outer midplane only)

Several different GPI cameras have been used for the outer midplane view since 2002, but by far the best quality data was taken by the Phantom 710 cameras since Dec. 2009, since these had higher framing rates than the earlier Phantom 7.3 (400 kHz vs. 250 kHz), and many more frames than the PSI cameras (30,000 vs. 300). All the Phantom 710 data since was also taken using the quartz fiberoptics bundles, which were free of neutron-gamma induced browning, and showed no significant browning up to 2016.

Excel spread sheets with a list of shots with Phantom 710 camera data were generated by Jim, including information about the GPI puff time, camera timing, and other parameters. There were four lists from Jim which I have, which are copied in the folder "CMod Phantom GPI shot lists" as "list #1…" etc. As far as I know, Phantom data continued to be taken from time-to-time until the end of C-Mod (Jim may have or could make more recent lists). Stewart's last visit to C-Mod was in July 2014.

list #1 - 1090904006 - 1100310028 (this starts with some 250 kHz shots)
list #2 - 1100630025 - 1110325032
list #3 - 1111297014 - 1120224034
list #4 - 1120613004 – 1121002033

Stewart went through all of the shot lists #1-4 to look for "good" GPI Phantom camera data, especially to find comparison shots for XGC1 runs. He looked at each GPI movie in these lists and each shot's scope data around the movie time (/home/zweben/scopes/4_col_mac.dat). He rated each shot A+ to C based on both image quality (noise level, signal level) and shot quality (steady-state conditions, smooth RF, good field line angle range in I/B). The whole shot list is at: "XGC shot list v.11 whole.txt" or "XGC shot list v.11 whole.qda" (Kaleidagraph file) in the folder "CMod Phantom GPI shot lists". There were 387 good (A or A+) shots identified in this process. These were also separately listed in shot order in "XGC shot list v.11 ordered.txt" and ""XGC shot list v.11 ordered.qda" files in the same folder. Simpler and clearer versions of this same 387 shot list are also in the same folder in other formats, e.g. pdf and Word. A simplified form of this list is in Appendix I.

This 387 list of good shots can be used for GPI database analysis, e.g. to evaluate the turbulence vs. current, density, RF power etc. The values of these parameters in Appendix 1 at the time of interest were read by hand from the scope traces, and so they may be some inaccuracies (they should be retrieved automatically if used in a database).

Videos of some of these shots can be seen on sz's web site, along with a link to the shot list at: http://w3.pppl.gov/~szweben/CMod2017/CMod2017.html. Also on this link is recently-made 6 minute (700 MB) annotated video with 16 sample shots and clips from their movies. The first two slides from this video are shown in Fig. 4.2. Videos from earlier C-Mod runs can also be found at: http://w3.pppl.gov/~szweben/.

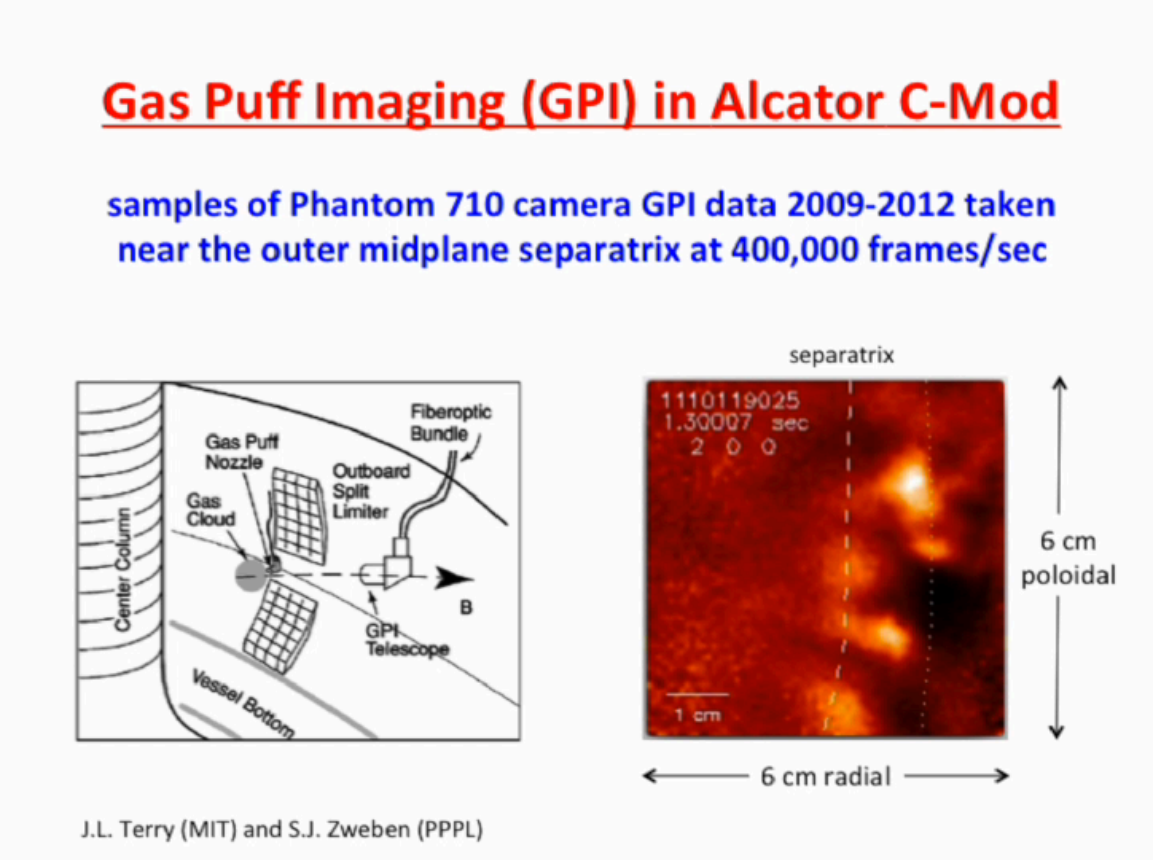

Fig. 4.2 – first slide from a 6 minute overview video of C-Mod GPI data

4.3 Best shots for initial XGC1 comparisons

The 387 shot list was examined for shots which could best be compared with the initial 0.8 MA C-Mod XGC1 run 1100223012. Six shots were selected for an initial comparison, as shown in the Table 1 below. This selection was based on plasma current, B field, RF power (avoiding nearby dropouts), and to some extent density, using shots

with a deuterium gas puff to make the comparisons simpler. A basic GPI camera turbulence analysis code (/home/zweben/phantom/phantom_XGC_15.pro) was run for each of these shots to compare the turbulence radial profiles with the XGC1 turbulence outputs. Initial results are in the file "GPI profiles @ 0.8 MA.pdf" in the folder "C-Mod GPI Guide". The resulting database "XGC database 0.8 MA.txt" and "…qda" is also there. Daren Stotler has also been working on this initial comparison.

shot	analysis nshot	Ip (MA)	Bt (T)	GPI start (s)	isep	Sig@sep	nl_04	outer gap (cm)	RF (MW)	GPI gas
1100223012	XGC	0.80	5.4	1.40	41	320.0	1.7	1.1	3.0	D
1100204002	39	0.81	5.4	0.798	32	169.0	0.70	1.5	3.5	D
1110120026	180	0.80	5.5	1.22	41	1201	1.4	1.1	2.8	D
1110120028	182	0.81	5.5	1.22	42	966.0	1.4	1.0	2.8	D
1110121018	185	0.81	5.5	1.15	42	132.0	1.4	1.1	4.0	D
1110121023	190	0.81	5.5	1.15	39	220.0	0.80	1.2	1.6	D

Table 1: initial comparison shots with XGC1 shot 1100223012

4.4 Additional comparisons of GPI camera data with XGC1

The initial comparison of GPI camera data with XGC1 using the shots shown in Table 1 has several limitations:

1) the shot 1100223012 simulated by XGC1 had a relatively low GPI gas puff and a low signal/noise level, and the 3D filament structure can be seen in the movies, which compromises the turbulence structure analysis, especially inside the separatrix

2) the B field angle was slightly misaligned with the GPI view, as can be seen in the tilt of the filaments inside the separatrix in the movie (best alignment ~0.9 MA/5.4 T)

3) this shot has strong RF heating and (as far as sz knows) does not have Langmuir probe data and so the density and temperature profiles in the SOL are uncertain

4) there is considerable spread in the turbulence results for the closest 6 shots, as shown in the analysis file mentioned in Sec. 4. 3, for reasons which are not yet clear. In particular, the separatrix location in the GPI may be varying more than expected from the present registration assignments (Jim should check).

For additional GPI-XGC1 comparisons, here are some suggestions (based on discussions with Daren and Michael Churchill):

1) start with an Ohmic shot with good GPI camera data, good GPI APD data, and good Langmuir probe turbulence and profile data, preferable one with several similar shots in the camera database. Ohmic shots will be free of RF, which is not in XGC1 and can cause undesirable fast poloidal flows in the SOL (see Sec. 6)

2) choose a shot with good B field alignment with the camera, based on an analysis of the B field line angle in the GPI field of view (see Sec. 8)

3) choose a shot with a good DEGAS 2 analysis of the GPI gas puff, either D or He or preferably both D and He puffs (on similar shots) for comparison

4) for RF shots, choose one without fast rotation induced by the RF, which can be judged by looking at the movie or doing a turbulence velocity analysis of the APDs. Fast rotation in the SOL is often too fast to be followed with the camera.

5) in any case, do a sensitivity analysis of the GPI database to estimate the uncertainty in the turbulence quantities to B, I, ne, RF etc. This would be an interesting study even without comparisons to XGC1.

5. Restoring and using the GPI camera data

For this section, we discuss only the Phantom 710 outer midplane camera data taken since 2009 (the X-region data is discussed in Sec. 6). The camera data is stored on the MDS+ tree in "SPECTROSCOPY::TOP.GPI.PHANTOM.frames", and backed up on an external Drobo 13 TB hard drive (in Jim's custody at MIT). The raw camera data is created in a proprietary Vision Research format (".cine"), and the process to retrieve and restore this data was written by Jim and is the same for all analysis codes and shots since 2009.

An example of an IDL code for restoring and viewing this GPI image data and making sample mpegs can be run using:

```
 /home/zweben/phantom/phantom710_mpeg12.pro
IDL> .r phantom710_mpeg12
IDL> get_phantom_data,1110120026,t1=1.22,t2=1.221,nframes=101,nplay=100,
        max=1300, norm=0,sm=1,med=1
```

These inputs have the following meaning:

1110120026 shot number
t1=1.22 – start time for retrieving data (sec), usually about 400 frames/msec
t2=1.221 – end time for retrieving data (sec), usually less than 10 msec after t1

nframes=101 - number frames to use in analysis (less than # of frames between t1 & t2)
nplay=100 - number of frames to play on screen and make into mpeg, less than nframes
max=1900 - maximum count level for un-normalized image shown on screen and mpeg
norm=0 - use 0 for un-normalized images, norm=1 for normalizing images by dividing each image by the average frame over nframes and scaling result from 0 to 2 (average of each pixel is 1); norm=2 scales normalized image from 0.5 to 1.5 instead
sm=1 - smoothing of frames in space by (sm,sm) pixels
med=1 - doing median of all frames in space over (med,med) pixels
mpeg=0 - makes mpeg of nframes of data if mpeg=1

program flow:
lines 29-89: GPI data is retrieved using code written by Jim Terry long ago
lines 91-99: image is flipped and 67 is subtracted to correct for zero-offset of camera; up in image is now upward in the machine, and left in image is inward toward the major axis; this creates image file: frames1(ipixel, jpixel, #), where ipixel=0-63, jpixel=0-63, and # is # of frames from 0 to the number from t1 to t2
lines 104-148: normalize and smooth data if those options chosen; the resulting image file used for movie analysis is nframes2(64,64,391) in this example
lines 152-170: play 64x64 movie of images in window0 between frames 0-nframes-1; median is done just before frame is shown
lines 174-184: plots window1 with average frame and smoothed average frame
lines 188-197: plots window2 with frames2(32,32,*) vs. frame number and real time
lines 197-209: rebin frames2 to movie1 to be x3 size, i.e. 192x192 for easier viewing
lines 213-375: find separatrix and limiter locations and convert into pixels on movie1 (see Sec. 7 for details on these conversions)
lines 378-451: play large movie1 in window3 over nplay frames, and make mpeg

Two output images from this code (window0 and window3) are shown in Fig. 5.1. The larger images take about 1 sec each to create, so if the input parameter nplay=100 this will take a couple of minutes to finish. The mpegs can be made with an mpeg=1 option but only on a work station at MIT which has a license for making mpegs. The runs for mpeg=0 can be made on any workstation.

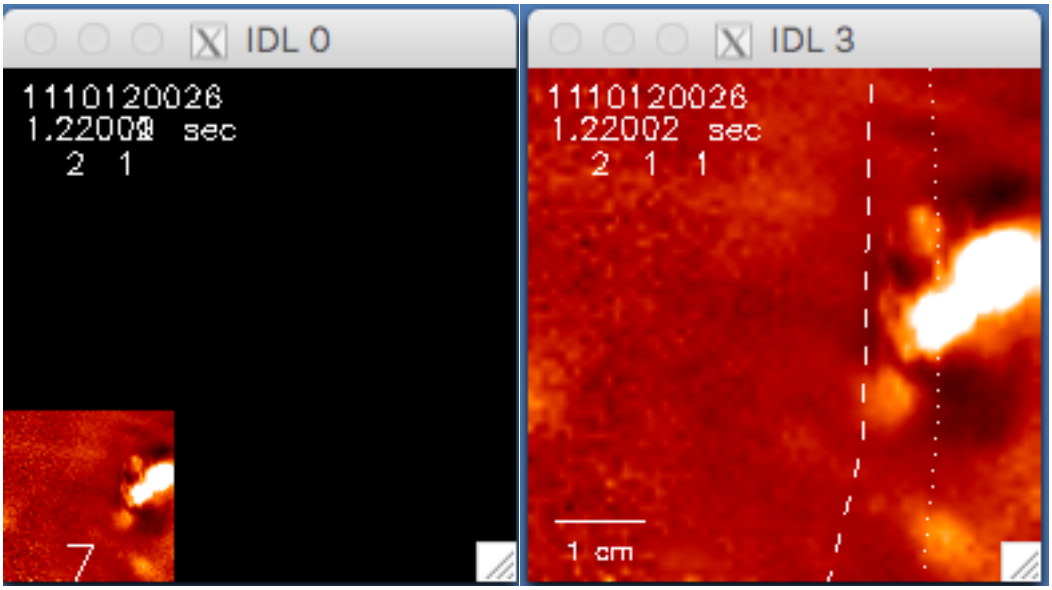

Fig. 5.1 - output images from phantom710_mpeg12.pro left 64x64, with norm=1; right 192x192 with overlaid separatrix (dashed) and limiter (dotted)

Another example of a recent code to restore and analyze C-Mod Phantom 710 data is also in /home/zweben/phantom:

```
IDL> .r phantom_XGC_15
IDL> xgc,nshot1=3,nshot2=3
```

This code does a relatively quick and simple GPI turbulence analysis specifically for the shots to be compared with XGC1 (see Table 1). The six shots of Table 1 and their start times t1 are already written into this code, along with default parameters such as:

nframes=1000 to analyze 1000 frames starting at t1 (e.g. nshot1=3 is shot 1110120026),
sm=3 - smoothing applied to image before analysis

norm=2 - normalizes data for turbulence analysis and plots results in range 0.5-1.5
iplot = 50 - sample column for plotting
istart = 10 - column to start turbulence analysis
iend = 50 - column to end turbulence analysis
ifwhm =12 - width of analysis region around separatrix for comparisons with XGC1
deltat = 0.003 - length of data to be restored, i.e. from t1 to t2=t1+deltat

The run above is completed in about 1 minute and outputs these analyses (see code itself for details of how these are calculated). Note that for this analyses the ipixel coordinate is assumed to be the same as the radial coordinate, since the local separatrix in

this image is nearly vertical as aligned with the isep line. There are some shots for which this is not the case, so this should be checked for each shot.

window0: restores the data as described just above and plays part of the 64x64 movie
window1: plots signals vs. time at (i1sep,32) at calculated separatrix location at vertical middle of image and (iplot,32) at chosen some other ipixel chosen as i=50
window2: plots the un-normalized average frame in 192x192 format with the separatrix and limiter overlaid, along with the calculated closest ipixel line to the separatrix and the radial (ipixel) analysis range shown as vertical dashes
window3: makes 8 plots of various analyzed quantities vs. horizontal ipixel coordinate
- time-averaed raw signal level in counts over istart to iend
- time-average raw signal level over all ipixels 0-63
- turbulence rms/mean
- turbulence autocorrelation time
- poloidal turbulence correlation length (cm)
- radial turbulence correlation length (cm)
- poloidal turbulence velocity (with error bars)
- radial turbulence velocity (with error bars)

windows7,8: plots 2d cross-correlation functions starting at (isep,32) and (iplot,32)
windows10,11,12: plots radial and poloidal profiles vs. time as vertical coordinate
window12: plots frequency spectra of (isep,32) and (iplot,32)
window20: plots poloidal and radial spatial cross-correlation functions vs. row & column
window25: re-plots some of window3

There are about 100 other Phantom 710 GPI analysis codes in sz's area, going back to 2009 at: /home/zweben/*.pro. Many of these are iterated versions of the same code, e.g. phantom_XGC_15. pro is the 15th version of this code. Sample outputs are of window3 and window9 are shown in Fig. 5.2.

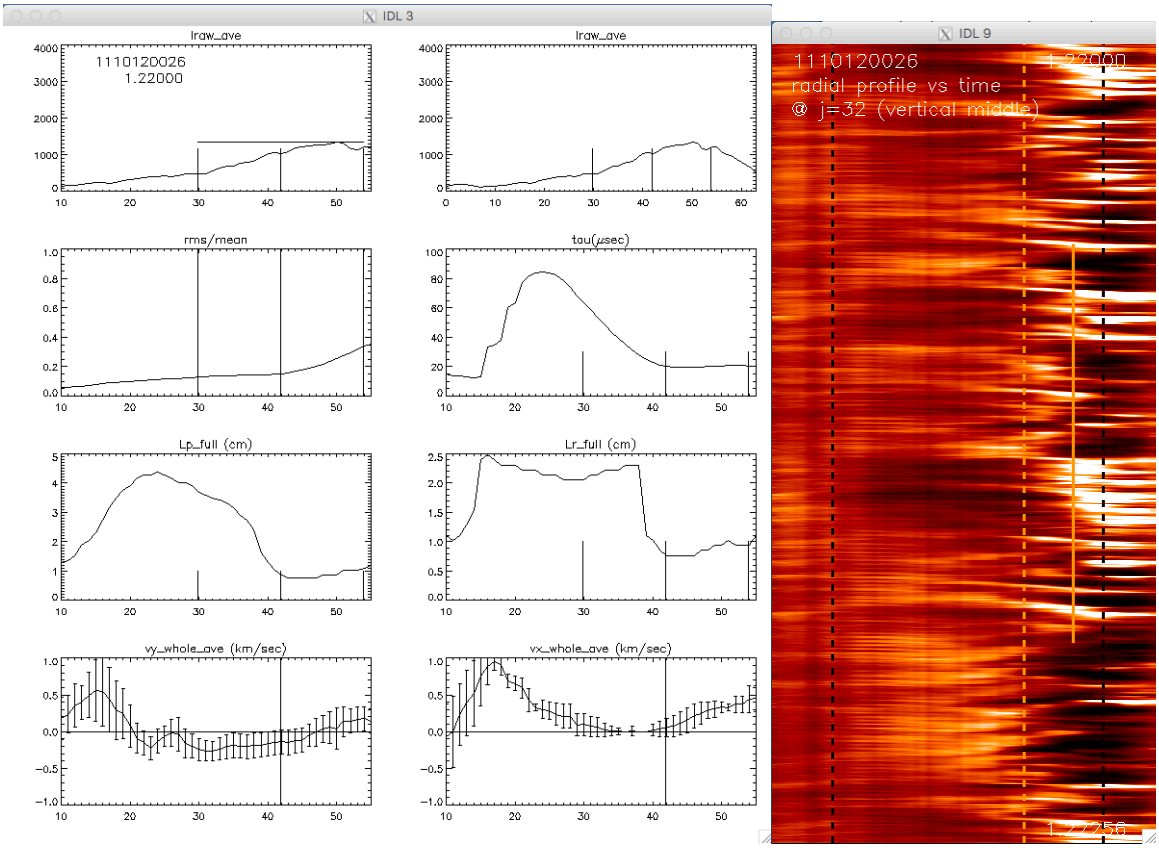

Fig. 5.2 – sample outputs from /home/zweben/phantom/phantom_XGC_15.pro

6. Hardware information for GPI cameras

These hardware issues are specific to the C-Mod GPI outer midplane and X-region Phantom 710 camera systems. For more general GPI diagnostic issues see our review paper at: Zweben, Terry et al, Rev. Sci. Instrum. 88, 041101 (2017), also copied into the Guide. This discussion starts with components nearest to the plasma and ends at the camera.

6.1 GPI gas puffers

The GPI gas puff to the midplane GPI camera view comes from a vertically aligned 4-hole nozzle mounted in a port on a shelf just below the outer midplane at the GPI image plane (see Fig. 6.1). The same 4-hole design has been in place since before 2009 and was intended to uniformly fill the GPI field of view with gas, but in practice the GPI signal brightness due to the puff was peaked near the vertical center of the image. Thus vertical variations in the average GPI brightness are due in part to the gas puff distribution, but can be normalized away by dividing by a time-averaged GPI frame. The X-region GPI puff was a single 1 mm capillary tube mounted in the divertor shelf as near

as possible to the X-region view. However, this puff nozzle was often far from the separatrix at that poloidal angle, so the neutral density from this puff varied significantly over the X-region image. Again, this variation can be removed by normalization.

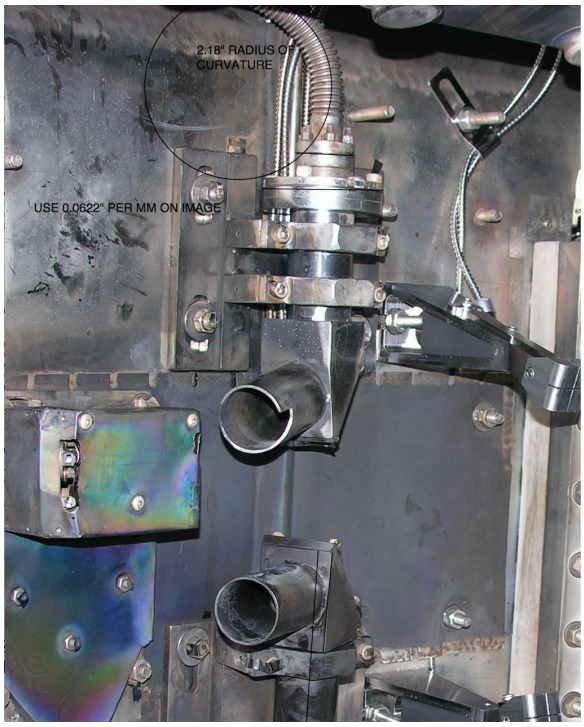

Fig. 6.1 - midplane GPI nozzle and field of view (left) and telescope (top right)

6.2 GPI in vessel telescopes

The outer midplane GPI telescope was mounted on the outer wall and pointed downward at fixed angle of 11º (Jim should confirm) toward the gas nozzles and the center of the GPI optical field of view. This angle was chosen to match a typical B field line angle at the outer midplane separatrix. A photo of this telescope is in Fig. 6.1 (the camera telescope is at the top, the APD telescope is below). The telescope contains several quartz lenses, and has a spatial resolution of ~1-2 mm at the object (GPI gas cloud) plane. This is comparable to the pixel resolution of (1/64)*6 cm ~ 1 mm for a typical imaging region at the outer midplane or X-region. No corrections for non-flatness of the optical imaging was ever used in GPI analysis, since these distortions were considered small.

There is always a potential for coating of this in-vessel optics, since there is no active shutter; this is why there is a cylindrical shield at the front end of the optics (see

Fig. 6.1 top). At the back end of this shield there is a stainless steel 45º mirror to direct the light upward to several quartz lenses (still in vacuum). This front-end mirror was usually cleaned by Jim at openings (Jim might comment). The image formed by the lenses is sent through a small vacuum window made of quartz and mounted at the end of the bellows which carries the quartz fiberoptics. This optics bundle is always in air, and the other end is connected to the camera at the top of the machine.

6.3 Quartz fiberoptic bundles and bellows

Both the outer midplane and X-region GPI cameras use two different 5 meter long, 0.158"x0.158" sized coherent quartz fiberoptic bundles to transmit the images to the cameras, which were installed inside the vessel in 2009 just prior to the start of the Phantom 710 camera usage. These bundles have a better transmission than glass and do not have radiation browning which darkened previous Schott glass bundles, but the quartz bundles have only 57x57 fibers (compared with 400x400 for the glass bundles). These were hand-made by Fiberoptic Systems Inc ($27k each, for specs see "FiberOptic Systems PPPL" and "quartz Bundle copy.ppt" in Guide). The fiber alignment is not perfect, but the end-to-end misalignments are at most ±1-2 fibers (see Fig. 6.2 for a similar bundle). There is also some mismatch between the 57 pixel bundle and the 64 pixel camera, so it is better to used normalized images for turbulence analysis to remove systematic spatial variations in overall transmission. Overall, we should not expect a spatial resolution of better than ~2/64 pixels, or ~2 mm in the final camera image, which is comparable to the optical resolution of the lenses in this system.

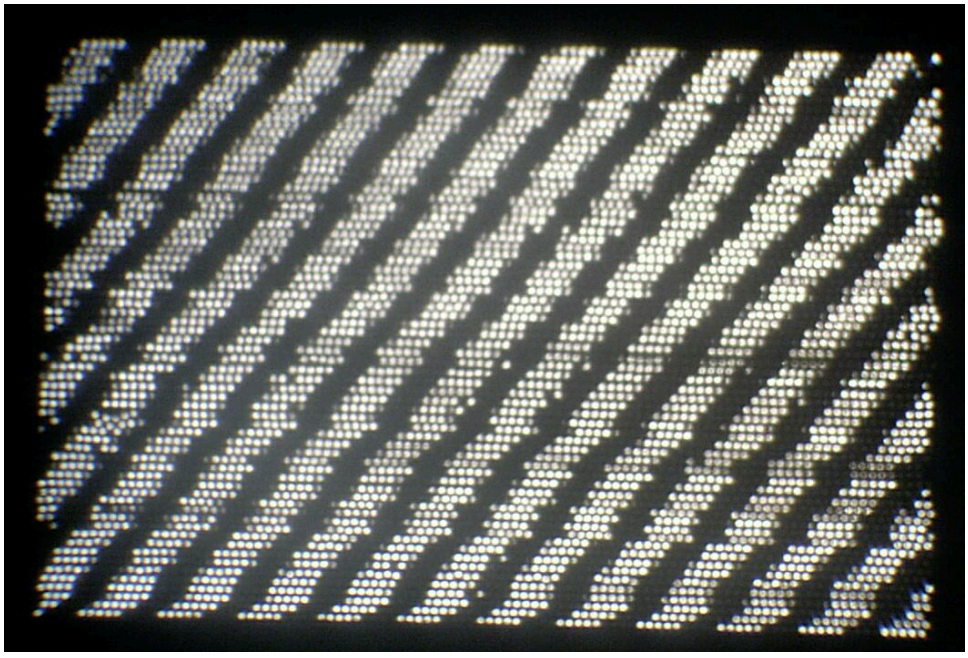

Fig. 6.2 quartz fiber end-to-end alignment quality typical for these bundles

The quartz bundles (and previously the Schott glass bundles) were enclosed in custom made vacuum bellows to transfer the light from inside the vessel to outside the vessel at the top of the machine. The interior end of this bellows can be seen at the top of Fig. 6.1. The other end of the bellows was attached to a flange at the top of the machine, and the fiberoptics came out of this end of the bellows and was connected in air to the camera, as shown in Fig. 6.3. The bellows never leaked (Jim confirm).

6.4 Ex-vessel optics and camera filters

The coherent fiber bundles were mounted on a manually controlled 3-d variable stage on a small optical bench on top of the machine, as shown in Fig. 6.3. The 0.158" square quartz optical bundle was imaged by a large 75 mm focal length commercial C-mount lens, focused to infinity for passage through the optical filter, and then x3 de-magnified and imaged onto the camera with a commercial 25 mm focal length C-mount lens. The Andover optical line transmission filters (656 nm ?? Jim put in widths if you can remember them nm FWHM or 587.6 nm ?? nm FWHM) were screwed onto the larger lens. This optic was covered by a black cloth during operation.

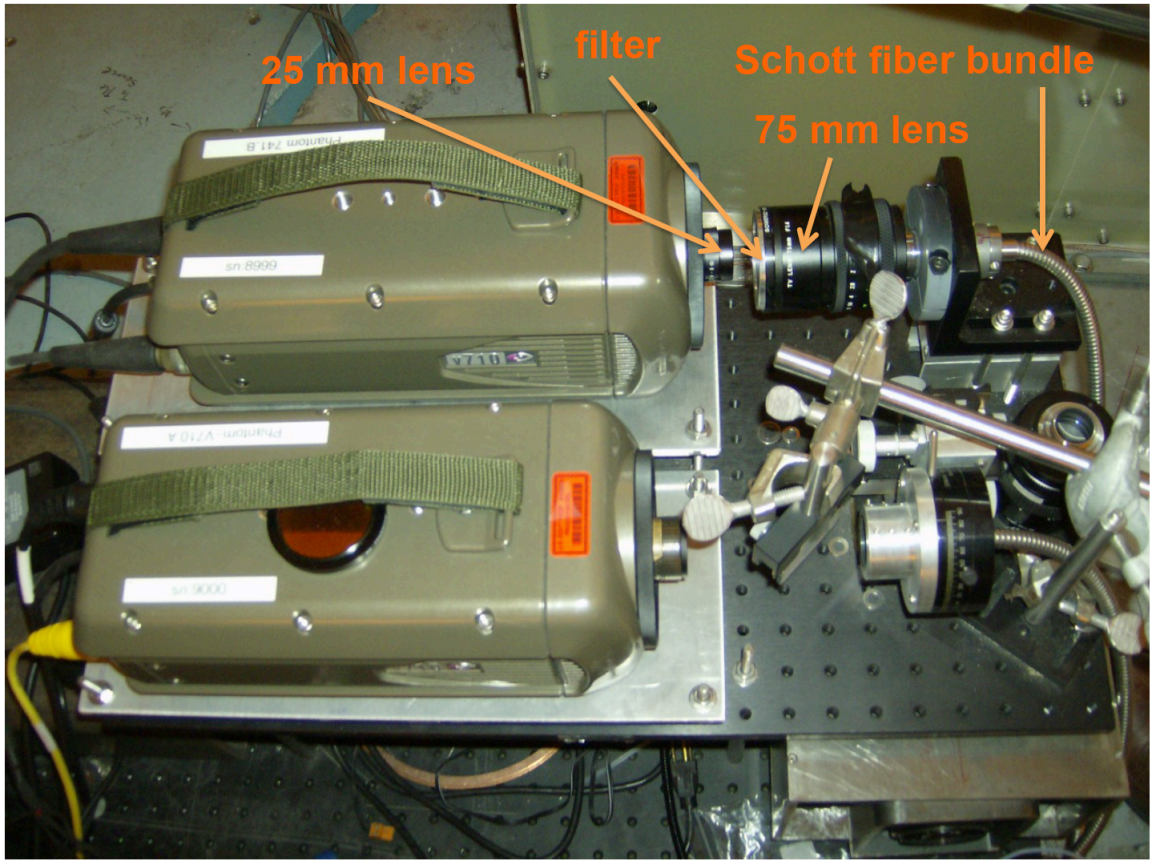

Fig. 6.3 ex-vessel GPI optics and 710 cameras

6.5 Phantom 710 camera characteristics

The Vision Research Phantom 710 cameras were bought in 2009 when these were first introduced to replace their Phantom 7.3 cameras. The spec sheets are in the Guide as "v710.pdf". These cameras worked well for about 8 years on C-Mod, but were sent back once or twice for minor repairs. There were no systematic changes in the camera performance over this time period, as far as we know.

The standard operating condition for both the outer midplane and X-region GPI cameras was 64x64 pixels at 397,000 frames/sec, which was the highest frame rate available at this pixel size. The actual camera exposure time was ~2.1 μsec/frame at this setting. Occasionally 128x128 pixel formats were used to check the location of the fiber bundle in the field of view, or slower framing rates were used to capture the whole shot. The camera sensor has 1280x800 pixels, most of which were never used for GPI (these are for slower frame rates). The spectral response curves for similar Phantom cameras are standard for a CMOS camera shown in the "Phantom Response curves.pdf" file in the Guide. The output is was digitized to 12 bit depth, most of which was not used in GPI (the maximum count level was typically 1500). The maximum number of frames recorded was limited by the time to transfer and store this data, typically a few minutes for 30,000 frames.

Based on the manufacturer's specs and some sample bench tests, we assumed that these cameras were linear in output vs. light level, flat in spatial response across the field of view, and had a time resolution of $\leq$ 2.5 μsec. Since the absolute light level is not important for GPI turbulence analysis, we assumed that there is no difference in camera response between Dalpha and HeI light.

7. Data analysis issues for GPI camera

This section describes data analysis issues for the Phantom 710 GPI cameras on C-Mod. A more general discussion of GPI analysis issues is in Zweben, Terry et al, Rev. Sci. Instrum. 88, 041101 (2017).

7.1 Camera offset, signal levels, and noise

The Phantom 710 outer midplane camera has a built-in positive output offset level of ~67±5 counts, apparently set so that the noise level at zero light can be seen more clearly. This level can be seen in shots with no plasma, and 67 is subtracted from all GPI signals before analysis. If this is not done, the relative fluctuation levels are slightly affected, but the turbulence correlation quantities are not. Good resulting signal levels are normally in the range ~500-1500 counts, i.e. far from the maximum available count level of 12 bits (4096). With this offset subtraction, the average the camera output with no light is ~10±10 counts, as can be seen in the (rare) shots which had a camera trigger but no plasma (e.g. 1100803021 @1.33 sec after a disruption).

The camera signal levels normally peak near the separatrix where the real GPI signal is largest, and fall well below 100 counts at the inner edge of the image (i=0). Examples of un-normalized frames taken from the code phantom710_mpeg12.pro are shown in Fig. 7.1, in which case the signal level at (32,32) is ~600. At the left the maximum bytscaled level is set to be max=600 counts (min=0), and at the right it is set to max=2000. There seems to be little or no clear turbulence signal below at the left side of the image below i=32, where there is still light but the spatial pattern is dominated by systematic variations in the fiberoptic transmission and/or camera pixel sensitivity. The real turbulence signal can be seen at the right to vary vs. time over a few frames (~5 μsec) and over ~5 pixel in space (~1 cm).

The signal level at which the turbulence can be distinguished from the random noise depends on the particular shot, and on the analysis techniques and goals. Time-dependent noise on the signals can come from the camera electronics, real statistical fluctuations in the photon signal from the GPI light, and electrical noise pickup from the environment (apparently rare). The pixel-to-pixel sensitivity is also slightly varying across the chip. *It is strongly advised to assess the signal/noise level in the image data by first looking at a short movie of the frames by eye before detailed analysis.* The real GPI signal should have no significant spatial variations between two adjacent pixels, since the spatial resolution of the optics is ~2 pixels (~2 mm), and there be no real signal variation in a single pixel from one frame to the next (2.5 μsec), since real turbulence (almost always) has an autocorrelation time of ≥5 μsec. Real turbulence can be seen as ~1 cm structures which move smoothly across the image over ~10's of μsec. Small average signals of ~100 counts can be seen during a shot, but the turbulence structures are difficult to identify. Clear turbulence signals can be seen by eye in the movies above a few hundred counts even in the un-normalized signals, although pixel-to-pixel and frame-to-frame noise due to statistical fluctuations are also visible. Clear turbulence structures are usually seen above ~1000 counts with relatively little noise. Looking at the frequency spectrum of a single pixel can also help to identify the noise level (noise is roughly flat vs. frequency).

In general, it is *highly desirable to normalize the images by a time-averaged frame over ~1 msec before turbulence analysis* in order to eliminate the systematic spatial variations due to the gas puff cloud itself, the fiberoptics and camera spatial irregularities, and the optical lens vignetting (i.e. smaller signals at the image edges). To further reduce noise when the signal/noise is low, it can be helpful to smooth and/or median the images over 3x3 pixels in space, and possibly also in by two frames in time.

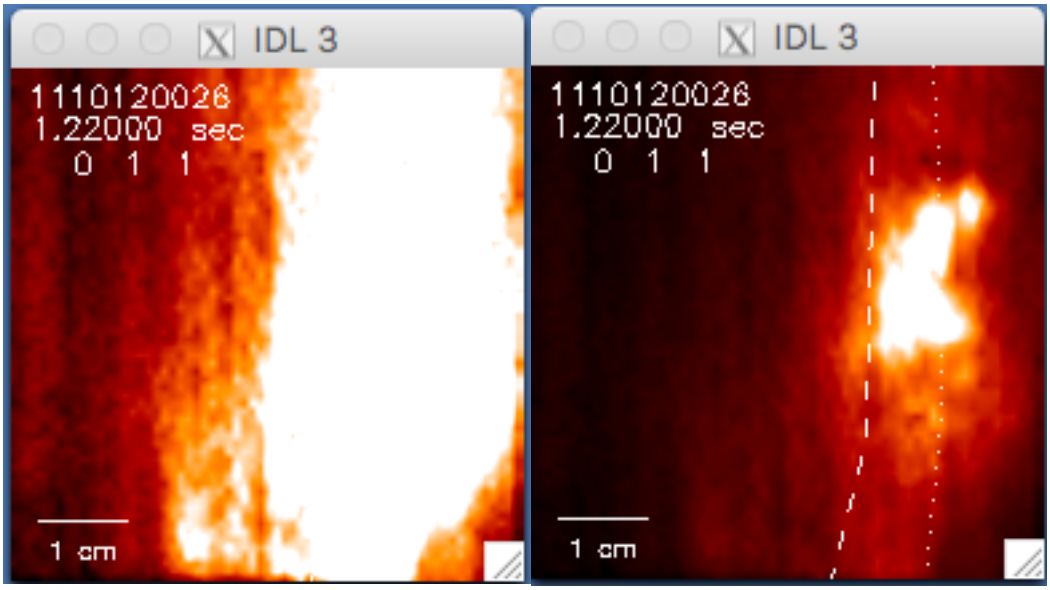

Fig. 7.1 - the same un-normalized image with max=600 (left) and 2000 (right)

7.2 Locating the GPI image in the machine

The bottom line for this section is that the GPI image coordinates and separatrix location are uncertain to a few mm radially, and care should be taken to review these coordinates with Jim Terry before finalizing the location of the GPI outer midplane camera data with respect to the separatrix.

The outer midplane GPI camera image location in machine coordinates was calibrated at most openings by Jim Terry using a back-lit white plate attached to local machine wall. The 4 corners of the fiberoptic bundle (as seen on the white plate were recorded in the MDS+ tree in C-Mod coordinates (R,z) as:

```
tr_corner = mdsvalue('\SPECTROSCOPY::TOP.GPI.PHANTOM.IMAGE_POS:TR_CORNER')
tl_corner = mdsvalue('\SPECTROSCOPY::TOP.GPI.PHANTOM.IMAGE_POS:TL_CORNER')
br_corner = mdsvalue('\SPECTROSCOPY::TOP.GPI.PHANTOM.IMAGE_POS:BR_CORNER')
bl_corner = mdsvalue('\SPECTROSCOPY::TOP.GPI.PHANTOM.IMAGE_POS:BL_CORNER')
```

where “tr”=top right, “bl”=bottom left, etc. There were also other registration values saved for each shot:

```
ang = mdsvalue('\SPECTROSCOPY::TOP.GPI.PHANTOM.IMAGE_POS:ang')
rt_pix = mdsvalue('\SPECTROSCOPY::TOP.GPI.PHANTOM.IMAGE_POS:rt_pix')
lt_pix = mdsvalue('\SPECTROSCOPY::TOP.GPI.PHANTOM.IMAGE_POS:lt_pix')
bot_pix = mdsvalue('\SPECTROSCOPY::TOP.GPI.PHANTOM.IMAGE_POS:bot_pix')
top_pix = mdsvalue('\SPECTROSCOPY::TOP.GPI.PHANTOM.IMAGE_POS:top_pix')
rotation = mdsvalue('\SPECTROSCOPY::TOP.GPI.PHANTOM.IMAGE_POS:rotation')
mirror_h_v = mdsvalue('\SPECTROSCOPY::TOP.GPI.PHANTOM.IMAGE_POS:mirror_h_v')
```

where rt_pix is the image pixel row at the right of the image aligned best with the bundle, top_pix is the image pixel row at the top of the image aligned best with the bundle, etc. rotation is the rotation angle of the bundle with respect to (R,z) coordinates, and ang and mirror describe the optics flip orientations.

The bundle corner coordinates originally input on 12/22/09 into were:

```
R1 = 85.7    ; bottom left
z1 = -5.85     ; bottom left
R2 = 91.3      ; bottom right
z2 = -6.00     ; bottom right
R3 = 86.2      ; top left
z3 = -0.05     ; top left
R4 = 91.7      ; top right
z4 = -0.15     ; top right
```

and these were used to define the bundle corners in the two GPI codes previously discussed in Sec. 5 (although the updated corners can be chosen in the code also). A comparison between the inferred separatrix and limiter location for a single frame using these 2009 coordinates and the updated "tr_corner" etc. coordinates for a 2011 shot is shown in Fig. 7.2. The updated separatrix/limiter locations are ~3 mm farther inward (to the left) than the 2009 coordinates. Probably the updated coordinates should be used in future analyses, subject to verification by Jim.

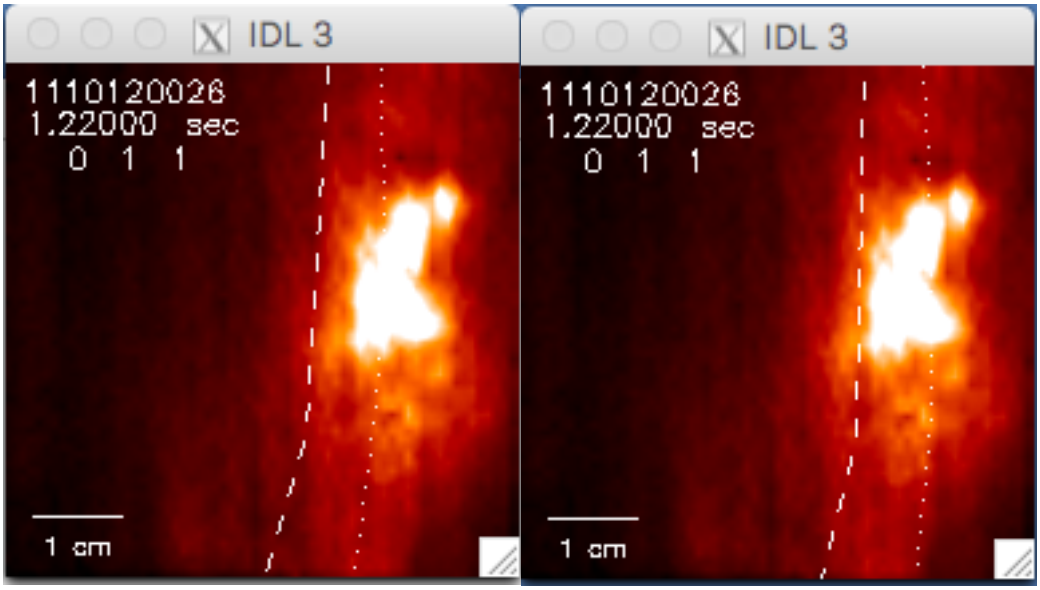

Fig. 7.2 separatrix/limiter locations with updated (left) and 2009 coordinates (right)

Another alignment issue in the outer midplane camera registration is that it is *assumed* in my (sz's) analysis, for either the 2009 or updated corner calibrations, that the camera pixel corners are coincident with the fiberoptic bundle coordinates. This was

assumed because the fiberoptic bundle location within the camera field of view was manually adjusted to be matched as well as possible with 64x64 pixel camera view by viewing the bundle in a 128x128 camera view during the camera set-up. This was of course never perfect, but was considered accurate to within about 1 mm in either direction. In principle, the bundle corners within the camera field of view were recorded in the parameters "rt_pix" etc as listed above and could have been used to slightly correct the image coordinates, but this was never done (at least by sz) for the outer midplane camera.

A third issue is the algorithm used in these analysis codes to map the separatrix and limiter coordinates onto the images using the image corner pixel coordinates. A simple interpolation algorithm was written by sz sometime around 2009 and incorporated in all outer midplane analysis codes since then (see either of the two codes of Sec. 5). This is not the same as the algorithm used by Jim, but was checked at some point to be very close (within 1 mm as I recall).

A final issue in the GPI camera alignment is the location of the separatrix itself, which was a topic of continued debate and analysis over the years in C-Mod. The (R,z) coordinates used in the GPI analysis codes by sz were:

```
rbbbs=mdsvalue('\efit_geqdsk:rbbbs', status=stat)
zbbbs=mdsvalue('\efit_geqdsk:zbbbs')
```

Jim would have to comment on the accuracy of these for any particular shots.

7.3 Magnetic field alignment angle with GPI view

All GPI systems are ideally designed to view the GPI gas cloud as much as possible along the local magnetic field line to optimize the spatial resolution of the field-aligned turbulence structures. The spatial blurring Δx due to angular misalignment is roughly (see GPI review RSI 2017, Eq. 1):

$$\Delta x \sim L_{II,cloud} \tan \theta_B$$

where $L_{II,cloud}$ is the length of the GPI gas cloud along B, and θ_B is the misalignment angle. A detailed study of the effect of this misalignment on the turbulence correlation structure for NSTX GPI is in Zweben et al, PoP 102509 (2017).

For the C-Mod outer midplane GPI there was never any direct measurement of $L_{II,cloud}$, which could only be done from a side view from another port. However, DEGAS 2 calculations by Daren Stotler based on the outer midplane puffer location for a "typical" C-Mod equilibrium gave $L_{II,cloud}$ (FWHM) ~ 6 cm [Zweben et al, Phys. Plasmas 16, 082505 (2009)]. If this is the case, then a spatial blurring of $\Delta x \sim 1$ cm, which is comparable to the usual correlation lengths measured by GPI is C-Mod, would occur at $\theta_B \sim 9.5^o$. It is plausible that the cloud length along B would also increase with larger distances away from the nozzle, and so be larger inside the separatrix than outside, and generally larger for shots with a larger outer gap. This effect will also be significant for

the outer midplane APD data, since the APD view was aligned along the toroidal direction and not along the local B field line (see Sec. 8).

For a quantitative analysis of this effect the local B field line angle in the GPI image plane should be calculate with EFIT, and the cloud size in 3d should be calculated with DEGAS 2 for the shot of interest. This would give an estimate of the spatial blurring due to B field misalignment, which up to now was assumed to be negligible. To my (sz) knowledge, this was not done routinely for GPI analysis in C-Mod, except for analysis of the APD data in Zweben et al, Phys. Plasmas 16, 082505 (2009). It would not be surprising if these misalignment angles varied significantly over the GPI field of view, as they do in NSTX (see Zweben et al, PoP 102509 (2017)).

7.4 Limitations of turbulence velocity analysis

The velocity of turbulent structures visible in the C-Mod GPI camera data was analyzed in several papers, e.g. Zweben et al, PPCF 025008 (2012), J.M. Sierchio, Rev. Sci. Inst. 87, 023502 (2016), and D.A. Russell et al., Phys. Plasmas 23, 062305 (2016). Both the poloidal and radial velocity of the turbulence are of significant physics interest, for example in evaluating zonal flows or Reynolds stress. However, their calculation from the GPI data has several important limitations and uncertainties, some of which are due to analysis techniques, some to hardware limitations, and some are unavoidable limitations to any 2d velocimerty based on image analysis.

Two main algorithms have been used to evaluate the turbulence velocity: a delayed-time cross-correlation method and a Fourier analysis method [see Sierchio et al for a comparison between them]. The time-delayed cross-correlation method was used most often in the camera data, for example in the code /home/zweben/phantom_XGC-15.pro discussed in Sec. 5. There the average turbulence velocity for a given time series was found by locating the peak of the time-delayed cross-correlation function in 2d, which gives an estimate of both the radial and poloidal turbulence velocity, averaged over the turbulence structure. This method tends to weight the largest structures most, and can not resolve counter-propagating structures, which can be done by the Fourier method. Time-dependent velocities such as zonal flows can be found by breaking up a ~10 msec time series into small sections (typically 30 μsec long) and evaluating the turbulence velocity vs. time for each segment by the cross-correlation method, as done in Zweben et al, PPCF 025008 (2012). The 2011 version of the zonal flow code used for that paper can be found at /home/zweben/phantom/phantom710_29.pro.

Very fast moving turbulence phenomena can not be measured well with the Phantom 710 camera since its maximum framing rate at 64x64 pixels was 400,000 frames/sec at 2.1 μsec exposure/frame. If the typical turbulent structure was ~1 cm in size (as it usually was), the it would be blurred and distorted by ~1 cm in the direction of motion at 5 km/sec. Typical zonal flow velocities in C-Mod from cross-correlation analysis were ≤1 km/sec, but poloidal velocities up to ≥5 km/sec were sometimes seen using the APDs during RF heating either in the SOL [R. Hong et al, PPCF 59, 105008

(2017)]. These high velocities can not easily be tracked by the cross-correlation method since the structures move ≥10 pixels/frame.

7.5 Examples of "B" shots in Phantom camera

As discussed in Sec. 4.2, there are at least 387 "good" Phantom 710 GPI camera shots in the years 2009-2012, as listed in the table in Appendix 1. These were the shots rated "A" and "A+" in the "XGC shot list v.11 whole" table in the Guide. Videos of 16 of these good shots can be seen in the highlights video at:
http://w3.pppl.gov/~szweben/CMod2017/CMod2017.html

Here we show examples of some types of shots which were rated "B", i.e. too poor for easy analysis, and give the reasons why they were rated poor (see also columns "analysis notes" and "movie grade" in the table "XGC shot list v.11 whole"). Images of single frames are in Fig. 7.3 made using phantom710_mpeg12.pro with norm=2, sm=1, med=1. Many of these are considered poor because the 3d parallel structure of the turbulence filaments are visible, extending to the left in the image from the SOL, which indicates poor localization of the GPI signal by the puff (i.e. too low a puff level). Some are poor because the I/B is too low or two high, making the alignment with the local B poor and implying poor spatial resolution of the turbulence. Some are poor because fast SOL motion was observed by eye in the movies either in the SOL or inside the separatrix, which could make velocity analysis difficult. A few had poor signal/noise or indistinct contrast of the turbulence, and a few had weird noise perhaps associated with RF pickup. Any of these might be analyzed further with some care and effort.

1091216034 - filaments extending horizontally left, implies puff level too low
1091216037 - filaments and too high B/I which makes them tilted
1100204003 - outer gap too small to see SOL clearly
1100212018 - small puff and filaments extending to left
1100310028 - small puff and filaments extending to left
1100819006 - ratty RF waveform, weird and tilted structures
1100819028 – strange fast SOL motion also inside separatrix
1120125005 – low signal and poor contrast for turbulence
1120703015 - fast motion near wall, ratty RF, low signal/noise inside separatrix

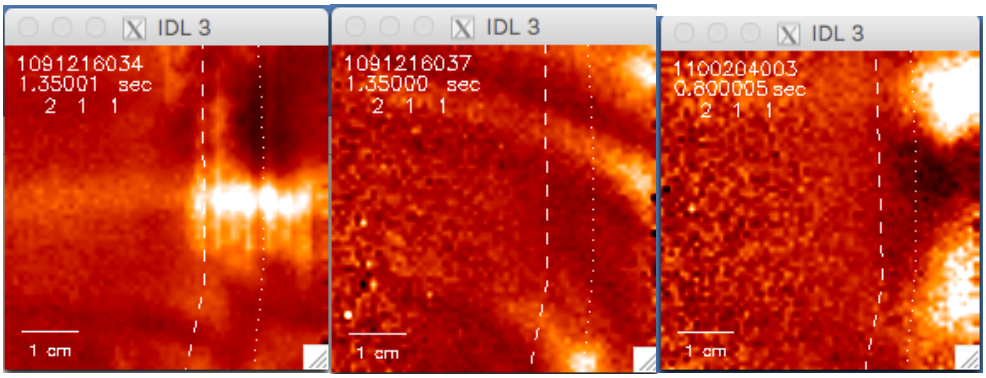

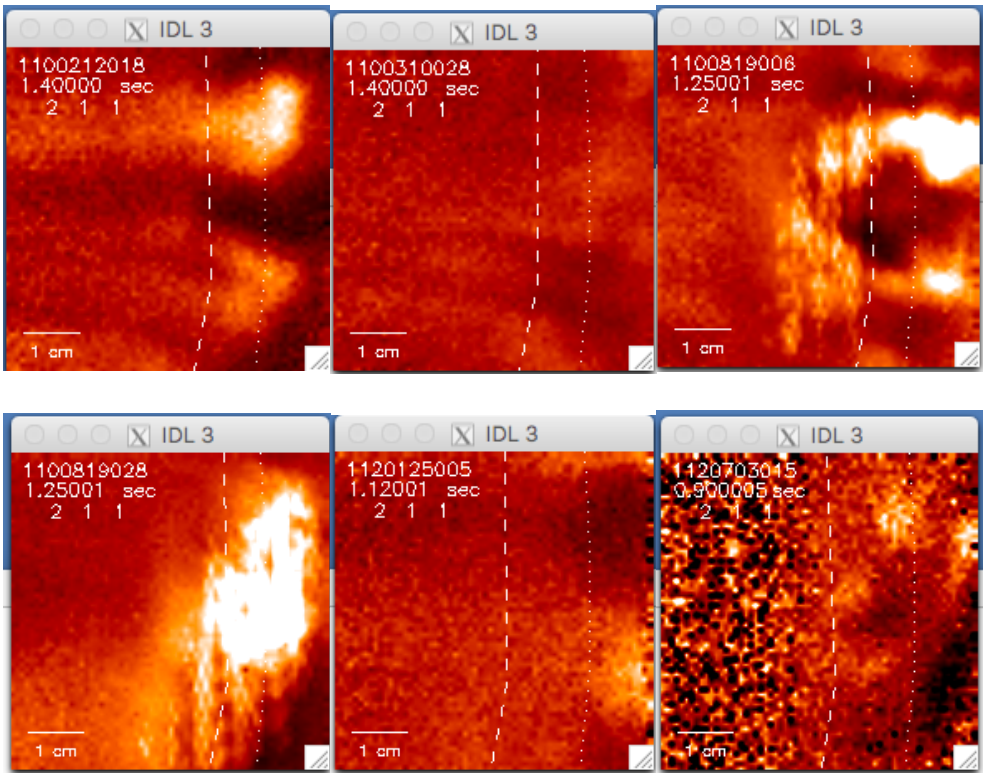

Fig. 7.3 examples of poor GPI camera data

9. Phantom 710 midplane camera vs. APDs (Jim comment as desired)

The APD (avalanche photodiode) midplane detector array partially overlaps the spatial viewing region of the Phantom 710 midplane camera, as shown in Fig. 9.1. The APD array views the plasma through a 9x10 discrete quartz fiber array pointed horizontally (0º vertically) at the GPI gas puff cloud, as shown at the bottom of Fig. 6.1. The APD data has several advantages with respect to the Phantom 710 camera data: better frequency response (2 MHz vs. 400 kHz sampling), better sensitivity to low-level signals, longer digitization period, and automatic recording. The disadvantages of the APD are its relatively few channels (some of which were broken over the years), smaller spatial coverage, larger distance between channels, and its significant misalignment with the B field line at the gas cloud, which compromises its spatial resolution of turbulent structures.

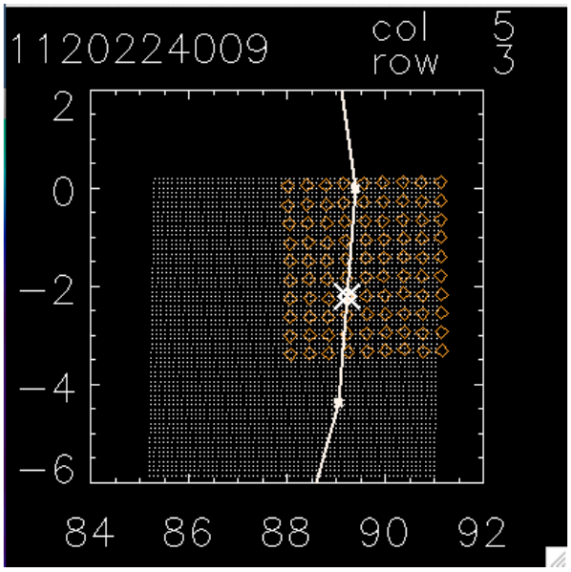

Fig. 9.1 APD array (orange circles) in camera field of view (2015 registration)

A detailed comparison between the APD GPI data and camera GPI data for a set of 2012 shots is described in the document "cam vs apd v.4.pdf" in the Guide, including a list of analysis programs used to compare these data. Typical results for the maximum cross-correlation between an APD channel and a camera pixel is shown in Fig. 9.2. The average cross-correlation coefficients is ~0.9 outside the separatrix, showing that these two detectors are basically viewing the same signal; however, the cross-correlation coefficients generally fall to ≤0.9 inside the separatrix, most likely because the camera signal/noise level becomes large there. Ideally, both systems should be used to analyze GPI data, bearing in mind the advantages and disadvantages of each.

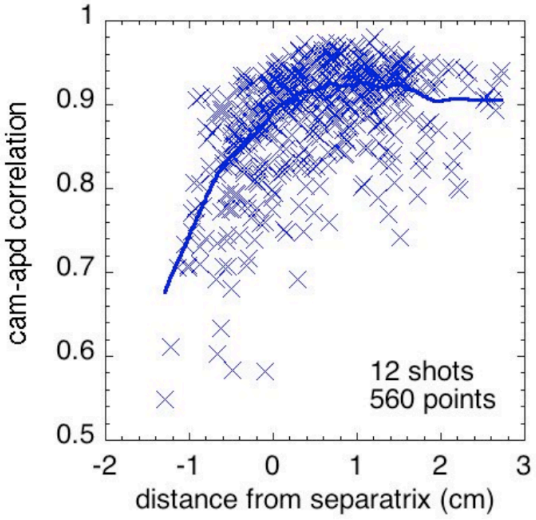

Fig. 9.2 cross-correlation between APD channel and camera pixel

9. Phantom 710 X-region GPI camera data

The purpose of the X-region GPI camera was to explore the structure of edge turbulence at a different location than the outer midplane. The X-region camera view was located as near as possible to the X-point of a LSN geometry shot, but was not designed to view the X-point itself. There were only two papers which discussed the X-region GPI camera data, Terry et al JNM 2009 and Zweben et al PoP 2013, the latter of which has more details of the hardware and a direct comparison between the midplane and X-region GPI images. More recently the filamentary turbulence in the X-point region in C-mod was viewed with passive imaging (Terry et al, Nucl. Materials and Energy 12, 989 (2017)).

An example of this X-region vs. outer midplane comparison is shown in Fig. 9.1, taken from the 2013. In general, the hardware and data analysis for the two systems was very similar, except for details of the image registration. The cameras were not directly synched with each other (Jim check), but the images could be compared at nearly the same time as in Fig. 10.1. The analysis codes for comparing the X-region and midplane region GPI cameras used in the 2013 paper are in the area /home/zweben/phantom, and the most recent version of the analysis code is 710_space_30.pro. This restores the separate image files and plots them frame-by-frame as shown for Fig. 9.1. An X-region shot list is in the Guide in the folder "CMod Phantom shot lists" as "X-point shot list…"

The biggest issue for the X-region camera data is the limited extent to which the turbulence is localized by the nearby gas puff. This is more of a problem than for the midplane data since the background signal levels are higher near the X-region, and the gas puff nozzle is farther from the imaging region. Thus the X-point images need to be analyzed carefully to insure that the 3d filament structure along the field lines is not domonating the turbulence analysis. Thus for initial comparisons with XGC1 the midplane data is recommended rather than the X-region GPI.

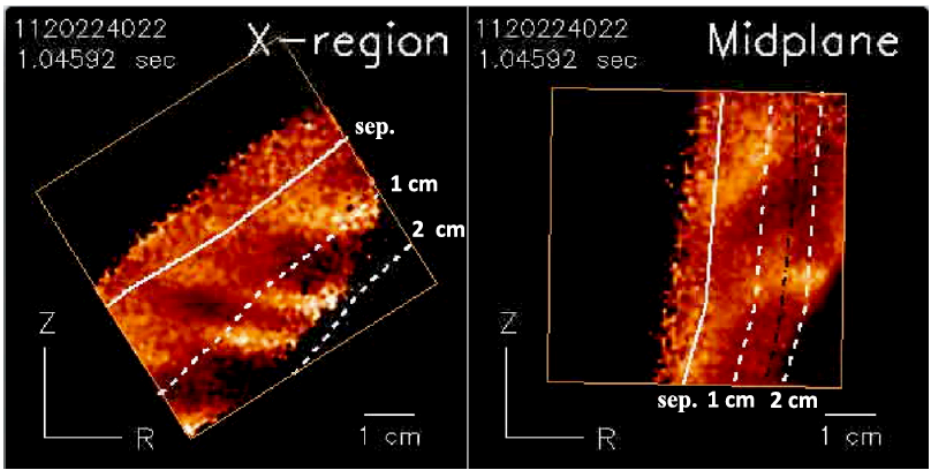

Fig. 10.1 X-region and midplane camera frames taken at the same time

10. List of good GPI camera shots 2009-2012

Also shown in various formats in folder "CMod phantom shot lists" in Guide.

shot	#	I (MA)	B(T)	Time(sec)	nl (cm-2)	gap(cm)	RF(MW)	GPI gas
1091216017	1	0.60	3.9	1.45	0.47	1.3	0.0	D
1091216018	2	0.60	3.9	1.45	0.55	1.3	0.0	D
1091216019	3	0.60	3.9	1.45	0.53	1.4	0.0	D
1091216020	4	0.60	3.9	1.45	0.69	1.4	0.0	D
1091216021	5	0.60	3.9	1.45	0.45	1.4	0.0	D
1091216023	6	0.40	2.6	1.45	0.45	1.4	0.0	D
1091216025	7	0.40	2.6	1.45	0.55	1.5	0.0	D
1091216026	8	0.40	2.6	1.45	0.55	1.4	0.0	D
1091216027	9	0.40	2.6	1.45	0.61	1.6	0.0	D
1091216028	10	1.0	5.2	1.45	0.80	1.4	0.0	D
1091216029	11	1.0	5.2	1.45	0.70	1.4	0.0	D
1091216030	12	1.0	5.2	1.45	0.68	1.4	0.0	D
1091216032	13	0.75	3.9	1.45	1.8	1.4	0.0	D
1091216033	14	0.75	3.9	1.45	1.7	2.2	0.0	D
1100120004	15	0.75	5.4	0.770	0.62	1.1	0.0	D
1100120005	16	0.75	5.4	0.770	0.65	1.2	0.0	D
1100120006	17	1.0	5.4	0.800	0.70	1.2	0.0	D
1100120008	18	1.0	5.4	0.800	0.64	1.2	0.0	D
1100120009	19	1.2	5.4	0.800	0.66	1.2	0.0	D
1100120011	20	1.2	5.4	0.800	0.70	1.4	0.0	D
1100120013	21	1.2	5.4	0.800	0.70	1.4	0.0	D
1100120014	22	1.2	5.4	0.800	0.60	1.4	0.0	D
1100120015	23	1.2	5.4	0.800	0.60	1.4	0.0	D
1100120018	24	0.80	3.6	0.800	0.38	1.3	0.0	D
1100120019	25	0.80	3.6	0.800	0.44	1.3	0.0	D
1100120020	26	0.80	3.6	0.800	0.50	1.4	0.0	D
1100120021	27	0.87	3.6	0.800	0.50	1.4	0.0	D
1100120022	28	0.89	3.6	0.800	0.55	1.4	0.0	D
1100120023	29	0.89	3.6	0.800	0.55	1.4	0.0	D
1100120024	30	0.89	3.6	0.800	0.55	1.5	0.0	D
1100120025	31	0.82	3.6	0.800	0.50	1.2	0.0	D
1100120026	32	0.82	3.6	0.800	0.50	1.2	0.0	D
1100120027	33	0.82	3.6	0.800	0.50	1.2	0.0	D
1100120028	34	0.88	3.6	0.800	0.55	1.5	0.0	D
1100120029	35	0.88	3.6	0.800	0.55	1.5	0.0	D
1100120030	36	0.88	3.6	0.800	0.55	1.5	0.0	D
1100120031	37	0.88	3.6	0.800	0.55	1.5	0.0	D
1100120032	38	0.88	3.6	0.800	0.55	1.5	0.0	D
1100204002	39	0.82	5.4	0.800	0.70	1.6	3.5	D
1100204006	40	1.0	5.4	0.800	0.70	0.90	0.0	D

1100204007	41	1.0	5.4	0.800	0.70	0.90	0.0	D
1100716003	42	0.80	5.4	1.30	0.55	1.0	0.0	D
1100716004	43	0.80	5.4	1.30	0.55	1.0	0	D
1100716006	44	0.80	5.4	1.30	0.55	1.0	0.0	D
1100716007	45	0.80	5.4	1.30	0.80	1.1	0.0	D
1100716008	46	0.80	5.4	1.30	0.80	1.1	0.0	D
1100716009	47	0.80	5.4	1.30	0.80	1.1	0.0	D
1100716010	48	0.80	5.4	1.30	1.0	1.2	0.0	D
1100716011	49	0.80	5.4	1.30	1.0	1.2	0.0	D
1100716012	50	0.80	5.4	1.30	1.2	1.2	0.0	D
1100716013	51	0.80	5.4	1.30	1.2	1.2	0.0	D
1100716014	52	0.80	5.4	1.30	1.4	1.3	0.0	D
1100716015	53	0.80	5.4	1.30	1.4	1.3	0.0	D
1100716016	54	0.55	5.4	1.30	0.40	1.1	0.0	D
1100716017	55	0.55	5.4	1.30	0.35	1.2	0.0	D
1100716018	56	0.55	5.4	1.30	0.53	1.2	0.0	D
1100716019	57	0.55	5.4	1.30	0.52	1.2	0.0	D
1100716020	58	0.55	5.4	1.30	0.60	1.3	0.0	D
1100716022	59	0.55	5.4	1.30	0.60	1.2	0.0	D
1100716023	60	0.55	5.4	1.30	0.60	1.3	0.0	D
1100716026	61	0.55	5.4	1.30	0.58	1.2	0.0	D
1100716027	62	0.55	5.4	1.30	0.45	1.2	0.0	D
1100721005	63	0.80	5.4	1.30	0.60	1.1	0.0	D
1100721007	64	1.1	5.4	1.30	0.77	1.2	0.0	D
1100721010	65	1.1	5.4	1.30	0.66	1.2	0.0	D
1100721011	66	1.1	5.4	1.30	0.66	1.2	0.0	D
1100721012	67	1.1	5.4	1.30	0.80	1.2	0.0	D
1100721014	68	1.1	5.4	1.30	0.70	1.2	0.0	D
1100721015	69	1.1	5.4	1.30	1.0	1.2	0.0	D
1100721025	70	1.0	5.4	1.30	0.86	1.3	0.0	D
1100721026	71	1.0	5.4	1.30	0.90	1.3	0.0	D
1100721027	72	1.1	5.4	1.30	0.94	1.3	0.0	D
1100721028	73	1.1	5.4	1.30	0.95	1.3	0.0	D
1100803004	74	0.80	4.0	1.30	0.70	1.1	0.0	He
1100803005	75	0.80	4.0	1.30	0.50	1.1	0.0	He
1100803006	76	0.80	4.0	1.30	0.50	1.1	0.0	He
1100803007	77	0.80	4.0	1.30	0.50	1.0	0.0	He
1100803008	78	0.80	4.0	1.30	0.70	1.1	0.0	He
1100803009	79	0.80	4.0	1.30	0.60	1.0	0.0	He
1100803011	80	0.80	4.0	1.30	0.80	1.0	0.0	He
1100803012	81	0.80	4.0	1.30	0.80	1.0	0.0	He
1100803013	82	0.80	4.0	1.30	0.90	1.1	0.0	He
1100803015	83	0.80	4.0	1.30	1.0	1.1	0.0	He
1100803020	84	0.80	4.0	1.30	1.0	1.0	0.0	He
1100803022	85	1.0	5.4	1.30	1.0	1.0	0.0	He

1100803023	86	1.0	5.4	1.30	1.0	1.0	0.0	He
1100803024	87	1.0	5.4	1.30	1.0	0.90	0.0	He
1100803027	88	1.0	5.4	1.30	1.0	0.90	0.0	He
1100803028	89	0.80	4.0	1.30	0.70	1.1	0.0	He
1100803029	90	0.80	4.0	1.30	0.50	1.1	0.0	He
1100803030	91	0.80	4.0	1.30	0.50	1.1	0.0	He
1100811003	92	0.80	6.0	1.25	0.60	0.90	0.0	He
1100811005	93	0.80	7.9	1.25	0.70	0.90	0.0	He
1100811006	94	0.80	7.9	1.25	0.50	0.30	0.0	He
1100811007	95	0.80	7.9	1.25	0.50	0.40	0.0	He
1100811009	96	0.80	7.9	1.25	0.70	0.50	0.0	He
1100811010	97	0.80	7.9	1.25	0.80	0.50	0.0	He
1100811011	98	0.80	7.9	1.25	0.80	0.50	0.0	He
1100811012	99	0.80	7.9	1.25	0.80	0.50	0.0	He
1100811013	100	0.80	7.9	1.25	1.0	0.50	0.0	He
1100811014	101	1.2	7.9	1.25	0.60	0.50	0.0	He
1100811015	102	1.2	7.9	1.25	0.60	0.50	0.0	He
1100811016	103	1.2	7.9	1.25	0.60	0.70	0.0	He
1100811017	104	1.2	7.9	1.25	0.80	0.60	0.0	He
1100811018	105	1.2	7.9	1.25	1.0	0.50	0.0	He
1100811019	106	1.2	7.9	1.25	1.2	0.50	0.0	He
1100811020	107	1.2	7.9	1.25	1.2	0.60	0.0	He
1100817009	108	1.1	5.7	1.00	1.1	1.1	3.2	D
1100817010	109	1.1	5.7	1.00	1.1	1.1	3.2	D
1100817011	110	1.1	5.7	1.00	1.1	1.1	2.0	D
1100817012	111	1.1	5.7	1.00	1.1	1.1	3.3	D
1100817013	112	1.1	5.7	1.00	1.1	1.1	3.5	D
1100817014	113	1.1	5.7	1.00	1.1	1.3	3.5	D
1100817015	114	0.80	5.7	1.00	1.1	1.1	2.0	D
1100817016	115	0.80	5.7	1.00	1.0	1.5	2.6	D
1100817017	116	0.80	5.7	1.00	0.90	1.3	3.5	D
1100817019	117	0.80	5.7	1.00	0.80	1.5	3.4	D
1100817020	118	0.80	5.7	1.00	0.80	1.5	3.4	D
1100817024	119	1.3	5.7	1.00	0.90	1.3	1.2	D
1100817025	120	1.3	5.7	1.00	0.90	1.2	1.2	D
1100819010	121	0.80	5.4	1.25	1.0	1.0	1.8	D
1100819011	122	0.80	5.4	1.25	1.7	0.90	1.4	D
1100819012	123	0.80	5.4	1.25	1.7	0.80	1.8	D
1100819013	124	0.80	5.4	1.25	1.8	1.0	2.1	D
1100819014	125	0.80	5.4	1.25	1.5	1.0	2.1	D
1100819015	126	0.80	5.4	1.25	1.5	1.0	2.1	D
1100824005	127	1.0	5.4	1.25	1.0	1.1	1.1	D
1100824006	128	0.90	5.4	1.25	2.2	0.90	1.3	D
1100824007	129	0.90	5.4	1.25	2.1	0.90	1.3	D
1100824008	130	0.90	5.4	1.25	2.1	1.0	1.3	D

1100824010	131	0.90	5.4	1.25	1.2	1.0	0.0	D
1100824011	132	0.90	5.4	1.06	1.0	1.2	0.50	D
1100824012	133	0.90	5.4	1.06	0.90	1.1	0.60	D
1100824013	134	0.90	5.4	1.06	1.0	1.1	0.60	D
1100824014	135	0.90	5.4	1.06	1.0	1.1	0.60	D
1100824015	136	0.90	5.4	1.06	0.90	1.1	0.80	D
1100824017	137	1.0	5.4	1.06	0.90	1.1	0.0	He
1100824019	138	1.1	5.4	1.06	1.0	1.1	0.0	He
1100824021	139	1.1	5.4	1.06	1.0	1.1	0.0	He
1100824022	140	1.1	5.4	1.06	1.0	1.1	0.0	He
1100824023	141	1.1	5.4	1.06	1.0	1.2	0.0	He
1100824024	142	1.1	5.4	1.06	1.0	1.1	0.0	He
1100824025	143	1.1	5.4	1.06	1.0	1.1	0.0	He
1100824026	144	1.1	5.4	1.06	1.0	1.1	0.0	He
1100824028	145	1.1	5.4	1.06	1.0	1.1	0.0	He
1100824029	146	1.1	5.4	1.06	1.0	1.1	0.0	He
1100824030	147	0.50	5.4	1.06	1.0	1.1	1.5	He
1100824031	148	0.50	5.4	1.06	1.0	1.2	2.0	He
1110114010	149	0.90	4.6	0.901	0.80	1.2	1.4	D
1110114011	150	0.90	4.6	0.901	0.77	1.2	0.0	D
1110114012	151	0.90	4.6	0.901	0.80	1.2	1.4	D
1110114013	152	0.80	4.0	0.901	0.74	1.3	1.0	D
1110114014	153	0.80	4.0	0.901	0.74	1.3	1.0	D
1110114015	154	0.80	4.0	0.901	0.74	1.4	1.8	D
1110114016	155	0.80	4.0	0.901	0.74	1.4	2.8	D
1110114017	156	0.80	3.9	0.901	0.72	1.4	2.8	D
1110114018	157	0.80	4.0	0.901	0.72	1.4	1.1	D
1110114019	158	0.80	4.0	0.901	0.72	1.4	1.3	D
1110114020	159	0.90	4.5	0.901	1.0	1.4	0.0	D
1110114021	160	0.90	4.5	0.901	1.0	1.4	1.0	D
1110114023	161	1.0	5.3	0.901	0.42	1.4	1.8	D
1110114025	162	1.0	5.3	0.901	0.65	1.2	1.8	D
1110114026	163	1.0	5.3	0.901	0.38	1.2	1.6	D
1110114027	164	1.0	5.3	0.901	0.38	1.2	1.8	D
1110114028	165	0.90	4.6	0.901	0.60	1.2	1.7	D
1110114032	166	0.90	4.6	0.901	0.40	1.2	1.8	D
1110114034	167	0.80	3.9	0.901	0.40	1.2	1.6	D
1110119025	168	0.80	5.5	1.30	1.4	1.2	2.0	D
1110119026	169	0.90	5.5	1.30	1.8	1.2	2.0	D
1110119027	170	0.90	5.5	1.30	1.6	1.2	2.0	D
1110119030	171	0.90	5.3	1.30	1.5	1.2	2.0	D
1110119031	172	0.85	5.5	1.23	1.4	1.2	2.0	D
1110119032	173	0.80	5.5	1.23	1.5	1.0	2.3	D
1110120018	174	0.82	5.4	1.20	1.5	1.1	2.1	D
1110120019	175	0.81	5.4	1.20	1.5	1.2	2.1	D

1110120020	176	0.81	5.4	1.20	1.5	1.2	2.2	D
1110120021	177	0.81	5.4	1.20	1.5	1.2	2.1	D
1110120024	178	0.81	5.5	1.20	1.4	1.0	2.3	D
1110120025	179	0.81	5.5	1.20	1.3	1.2	2.5	D
1110120026	180	0.81	5.5	1.20	1.3	1.2	2.5	D
1110120027	181	0.81	5.5	1.20	1.4	1.2	2.5	D
1110120028	182	0.81	5.5	1.25	1.4	1.2	2.8	D
1110120029	183	0.81	5.5	1.25	1.4	1.2	2.4	D
1110120030	184	0.82	5.5	1.20	1.5	1.2	2.2	D
1110121018	185	0.82	5.5	1.25	1.5	1.1	2.7	D
1110121019	186	0.82	5.5	1.25	1.5	1.1	3.4	D
1110121020	187	0.82	5.5	1.25	1.5	1.1	2.6	D
1110121021	188	0.82	5.5	1.25	1.5	1.1	2.6	D
1110121022	189	0.81	5.5	1.23	1.2	1.2	1.5	D
1110121023	190	0.81	5.5	1.25	1.2	0.20	3.4	D
1110121024	191	0.81	5.5	1.25	1.2	1.2	1.5	D
1110121025	192	0.81	5.5	1.25	1.2	1.2	1.5	D
1110121026	193	0.81	5.5	1.22	1.5	1.2	2.4	D
1110121028	194	0.81	5.5	1.22	1.0	1.2	2.3	D
1110121029	195	0.81	5.5	1.22	1.4	1.2	3.2	D
1110121030	196	0.81	5.5	1.22	1.0	1.2	2.3	D
1110121031	197	0.80	5.5	1.25	1.7	1.2	2.3	D
1110127005	198	0.80	5.5	1.13	0.90	0.80	0.50	He
1110127006	199	0.80	5.5	1.13	0.90	1.8	0.50	He
1110127007	200	0.81	5.4	1.13	0.70	0.90	0.40	He
1110127008	201	0.81	5.4	1.13	0.70	1.8	0.40	He
1110127010	202	0.81	5.4	1.13	0.80	0.90	0.90	He
1110127011	203	0.81	5.4	1.13	0.80	1.8	0.80	He
1110127012	204	0.81	5.4	1.13	0.80	1.8	0.80	He
1110127013	205	0.81	5.4	1.13	0.80	0.90	0.80	He
1110127014	206	0.81	5.4	1.13	0.80	1.8	0.80	He
1110127015	207	0.81	5.4	1.13	0.80	1.8	0.80	He
1110127019	208	1.0	4.6	1.13	0.60	0.80	0.0	He
1110127020	209	1.0	4.6	1.13	0.60	0.80	0.0	He
1110127027	210	0.70	5.4	1.13	0.60	0.80	0.0	He
1110127028	211	0.70	5.4	1.13	0.60	0.80	0.0	He
1110218003	212	0.80	5.5	1.10	0.35	2.4	0.0	He
1110218004	213	0.80	5.5	1.10	0.35	1.7	0.0	He
1110218017	214	0.60	5.5	1.10	0.35	1.7	0.0	He
1110218018	215	0.80	5.5	1.10	0.35	1.7	0.0	He
1110310006	216	1.0	5.4	1.25	1.0	2.0	2.1	D
1110310007	217	1.2	5.4	1.25	1.3	1.7	2.1	D
1110310008	218	0.80	5.4	1.25	0.90	1.7	1.1	D
1110310009	219	0.80	5.4	1.25	0.90	1.7	1.1	D
1110310010	220	0.60	5.4	1.25	0.75	1.7	1.1	D

1110325011	221	0.70	3.5	1.25	1.0	2.0	0.0	He
1110325012	222	0.70	3.5	1.25	0.90	1.7	1.0	He
1110310020	223	0.45	3.5	1.25	0.70	1.7	1.1	He
1110310025	224	0.70	3.5	1.25	0.90	1.7	1.1	He
1110310010	225	0.60	5.4	1.25	1.0	1.5	2.0	He
1111208002	226	0.55	5.4	0.900	0.40	1.3	0.0	He
1111208003	227	0.55	5.4	0.900	0.40	1.0	0.0	He
1111208020	228	0.80	5.4	0.900	0.70	1.1	0.0	He
1120207004	229	1.0	5.3	0.850	1.3	1.7	0.65	He
1120207006	230	1.0	5.3	0.850	1.3	0.90	0.70	He
1120207007	231	1.0	5.3	1.40	2.0	1.3	1.5	He
1120207014	232	1.0	5.3	1.00	2.0	0.90	2.6	He
1120207015	233	1.0	5.3	1.00	0.80	1.2	0.40	He
1120207022	234	1.0	5.3	1.30	0.70	1.2	0.0	He
1120207023	235	1.0	5.5	1.45	0.70	1.2	0.0	He
1120207028	236	1.0	5.5	1.20	0.90	1.8	2.0	He
1120207029	237	1.0	5.5	1.30	1.0	2.0	1.8	He
1120207030	238	1.0	5.5	1.30	1.0	2.0	1.8	He
1120207031	239	1.0	5.5	1.30	1.0	2.0	0.40	He
1120207032	240	1.0	5.5	1.30	0.90	2.0	0.70	He
1120209003	241	1.0	5.2	0.900	0.60	1.1	1.5	He
1120209004	242	1.0	5.2	0.900	0.60	1.4	1.6	He
1120209012	243	1.0	5.2	1.20	0.40	1.3	2.3	He
1120210007	244	0.80	5.4	1.45	0.30	2.2	0.0	He
1120210008	245	0.80	5.4	1.45	0.22	2.2	0.0	He
1120210010	246	0.80	5.4	1.45	0.30	2.2	0.0	He
1120210011	247	0.80	5.4	1.45	0.60	2.2	0.0	He
1120210012	248	0.80	5.4	1.45	0.50	2.1	0.0	He
1120210013	249	0.80	5.4	1.45	0.50	2.2	0.0	He
1120210014	250	0.80	5.4	1.45	0.50	2.1	0.0	He
1120210015	251	0.80	5.4	1.45	0.50	2.2	0.0	He
1120210020	252	0.80	5.4	1.45	0.60	2.2	0.0	He
1120210021	253	0.80	5.4	1.45	0.60	2.2	0.0	He
1120210026	254	0.80	5.4	1.45	0.80	2.4	0.0	He
1120210031	255	0.80	5.4	1.45	0.50	2.2	0.0	He
1120210032	256	0.80	5.4	1.45	0.70	2.2	0.0	He
1120216004	257	1.1	5.6	1.00	0.25	1.7	0.0	He
1120216006	258	1.1	5.6	1.00	0.40	1.7	0.0	He
1120216011	259	1.1	5.6	1.00	0.70	1.7	0.0	He
1120216012	260	1.1	5.5	1.00	1.7	1.7	0.0	He
1120216013	261	1.1	5.5	1.00	0.90	1.7	0.0	He
1120216014	262	1.1	5.5	1.00	1.0	1.7	0.0	He
1120216017	263	1.1	5.5	1.00	1.8	1.7	0.0	He
1120216025	264	0.55	5.5	1.00	0.40	1.7	0.0	He
1120216028	265	0.55	5.5	1.00	0.30	1.7	0.0	He

1120216030	266	0.80	5.5	1.00	0.50	1.7	0.0	He
1120216031	267	0.80	5.5	1.00	0.50	1.7	0.0	He
1120217003	268	0.80	5.4	1.40	0.60	1.1	0.0	He
1120217007	269	0.80	5.4	1.40	0.60	1.1	0.0	He
1120217008	270	0.80	5.4	1.40	0.60	1.1	0.0	He
1120217009	271	0.80	5.4	1.40	0.60	1.1	0.0	He
1120217010	272	0.80	5.4	1.40	0.60	1.1	0.0	He
1120217011	273	0.80	5.4	1.40	0.70	1.1	0.0	He
1120217012	274	0.80	5.4	1.40	0.80	0.70	0.0	He
1120217013	275	0.80	5.4	1.40	0.80	0.80	0.0	He
1120217014	276	0.80	5.4	1.40	0.90	0.80	0.0	He
1120217015	277	0.80	5.4	1.40	0.90	0.70	0.0	He
1120217016	278	0.80	5.4	1.40	1.0	0.70	0.0	He
1120217017	279	0.80	5.4	1.40	1.0	1.2	0.0	He
1120217018	280	0.80	5.4	1.40	1.0	1.2	0.0	He
1120217019	281	0.80	5.4	1.40	1.0	1.2	0.0	He
1120217020	282	0.80	5.4	1.40	1.4	1.2	0.0	He
1120217021	283	0.80	5.4	1.40	1.4	1.2	0.0	He
1120217022	284	0.80	5.4	1.40	1.3	1.2	0.0	He
1120217025	285	0.80	5.4	1.40	1.4	1.2	0.0	He
1120217026	286	0.80	5.4	1.40	1.4	1.2	0.0	He
1120217027	287	0.80	5.4	1.40	0.90	1.2	0.0	He
1120217028	288	0.80	5.4	1.40	0.70	1.1	0.0	He
1120223031	289	1.0	5.4	0.950	1.2	1.5	1.2	He
1120223032	290	1.0	5.4	0.850	0.60	1.5	1.0	He
1120223033	291	1.0	5.4	0.950	1.2	1.4	1.0	He
1120223034	292	1.0	5.4	0.950	1.0	1.5	1.9	He
1120224002	293	1.0	5.4	0.750	0.50	1.7	1.2	He
1120224003	294	1.0	5.4	0.900	0.65	1.6	1.6	He
1120224004	295	1.0	5.4	0.900	1.9	1.7	2.6	He
1120224005	296	1.0	5.4	0.750	1.8	1.5	2.5	He
1120224006	297	1.0	5.4	0.750	0.70	1.5	2.5	He
1120224007	298	1.0	5.4	0.950	0.60	1.4	2.0	He
1120224008	299	1.0	5.4	0.850	0.70	1.7	2.5	He
1120224009	300	0.90	4.6	0.850	0.65	1.3	2.4	He
1120224010	301	0.90	4.6	0.850	0.70	1.3	3.0	He
1120224011	302	1.1	6.0	0.850	0.80	1.2	3.0	He
1120224012	303	1.0	6.0	0.850	0.70	1.1	3.2	He
1120224013	304	1.0	6.0	0.850	0.80	1.2	3.6	He
1120224014	305	1.0	6.0	0.850	0.80	1.2	3.6	He
1120224015	306	1.0	6.0	0.849	0.70	1.2	3.7	He
1120224016	307	1.0	6.0	0.850	0.70	1.2	0.0	He
1120224018	308	1.0	5.3	0.920	0.40	1.2	1.4	He
1120224019	309	1.0	5.3	0.920	0.70	1.2	1.7	He
1120224020	310	1.0	5.3	0.900	0.70	1.2	2.4	He

1120224022	311	1.0	5.3	1.10	0.60	1.2	2.7	He
1120224023	312	1.0	5.3	1.15	0.90	1.5	3.0	He
1120224024	313	1.0	5.3	1.15	1.0	1.5	2.9	He
1120224025	314	1.0	5.3	1.15	1.0	2.0	3.0	He
1120224026	315	1.1	6.0	1.15	0.70	1.4	3.0	He
1120224027	316	0.90	4.6	1.15	0.70	1.4	3.0	He
1120224028	317	0.90	4.6	1.19	1.0	1.5	2.9	He
1120224029	318	0.90	4.6	1.19	1.5	1.5	3.9	He
1120224030	319	0.90	4.6	1.19	1.4	1.3	3.6	He
1120224032	320	0.80	5.4	1.30	0.70	1.8	3.9	He
1120224033	321	0.80	5.4	1.30	0.70	1.8	3.9	He
1120224033	322	0.80	5.4	1.30	0.70	1.8	2.0	He
1120711001	323	0.55	5.4	1.30	0.60	1.2	0.0	He
1120711002	324	0.55	5.4	1.30	0.40	1.2	0.0	He
1120711003	325	0.55	5.4	1.30	0.50	1.4	0.0	He
1120711004	326	0.55	5.4	1.30	0.50	1.2	0.0	He
1120711005	327	0.55	5.4	1.30	0.50	1.4	0.0	He
1120711006	328	0.55	5.4	1.30	0.60	1.1	0.0	He
1120711007	329	0.55	5.4	1.30	0.60	1.1	0.0	He
1120711008	330	0.55	5.4	1.30	0.75	1.1	0.0	He
1120711009	331	0.55	5.4	1.30	0.75	1.1	0.0	He
1120711010	332	0.55	5.4	1.30	0.95	1.1	0.0	He
1120711011	333	0.55	5.4	1.30	0.80	1.1	0.0	He
1120711012	334	0.55	5.4	1.30	0.80	0.90	0.0	He
1120711014	335	0.80	5.4	1.30	0.50	0.80	0.0	He
1120711015	336	0.80	5.4	1.30	0.50	0.90	0.0	He
1120711019	337	0.80	5.4	1.30	0.70	0.90	0.0	He
1120711020	338	0.80	5.4	1.30	0.70	0.90	0.0	He
1120711021	339	0.80	5.4	1.30	0.95	0.90	0.0	He
1120711022	340	0.80	5.4	1.30	1.0	1.0	0.0	He
1120711023	341	0.80	5.4	1.30	1.0	1.0	0.0	He
1120711024	342	0.80	5.4	1.30	1.0	1.0	0.0	He
1120711025	343	0.80	5.4	1.30	1.2	0.90	0.0	He
1120711027	344	0.80	5.4	1.30	1.2	0.70	0.0	He
1120712022	345	0.73	4.2	1.45	1.9	0.40	0.0	He
1120712023	346	0.73	4.2	1.45	1.3	0.10	0.0	He
1120712024	347	0.73	4.2	1.45	1.0	0.40	0.0	He
1120712025	348	0.73	4.2	1.45	1.8	0.20	0.0	He
1120712026	349	0.73	4.2	1.45	2.2	0.30	0.0	He
1120712027	350	0.73	4.2	1.45	2.2	0.30	0.0	He
1120712028	351	0.73	4.9	1.45	1.6	0.10	0.0	He
1120712029	352	0.73	4.9	1.45	1.3	0.10	0.0	He
1120718014	353	1.0	5.4	1.30	0.50	2.1	0.0	He
1120718015	354	1.0	5.4	1.30		2.1	0.0	He
1120718016	355	1.0	5.4	1.30	0.50	2.0	0.0	He

1120718017	356	1.0	5.4	1.30	0.50	2.0	0.0	He
1120718026	357	1.0	5.4	0.75	0.70	2.0	1.1	He
1120731013	358	0.80	5.4	1.30	1.0	1.6	2.5	He
1120731015	359	0.80	5.5	1.30	1.6	1.4	3.7	He
1120731017	360	0.80	5.5	1.30	1.0	1.3	0.90	He
1120731018	361	0.90	5.6	1.30	1.3	1.0	0.80	He
1120731019	362	0.90	5.6	1.30	1.4	0.90	1.0	He
1120731023	363	0.80	5.4	1.30	1.7	1.7	2.4	He
1120731024	364	0.80	5.4	1.30	1.8	1.6	2.3	He
1120815016	365	0.90	5.6	1.30	1.6	1.3	3.0	He
1120815018	366	0.90	5.6	1.30	1.5	1.5	2.5	He
1120815019	367	0.90	5.6	1.30	1.6	1.4	3.0	He
1120815020	368	0.90	5.6	1.30	1.3	1.3	3.0	He
1120905002	369	0.80	5.4	0.800	1.3	1.7	2.9	He
1120905003	370	0.80	5.4	0.800	1.3	1.8	3.0	He
1120905004	371	0.80	5.4	0.800	1.0	1.9	1.5	He
1120905005	372	0.80	5.4	0.800	1.3	1.9	3.0	He
1120905006	373	0.80	5.4	0.800	1.3	1.0	1.5	He
1120905007	374	0.80	5.4	0.800	1.3	1.7	1.5	He
1120905008	375	0.80	5.4	0.800	1.3	1.7	2.0	He
1120905011	376	0.80	5.4	0.800	1.2	1.7	3.0	He
1120918005	377	0.80	5.4	1.15	1.0	2.0	1.5	He
1120918006	378	0.80	5.4	1.15	1.0	2.0	1.5	He
1120918007	379	0.80	5.4	1.15	1.0	2.0	1.5	He
1120918008	380	0.80	5.4	1.15	1.0	1.7	1.3	He
1120921004	381	1.1	5.4	1.40	0.90	1.6	3.4	He
1120921005	382	1.1	5.4	1.40	0.90	1.6	1.8	He
1120921006	383	1.1	5.4	1.40	0.90	1.6	1.6	He
1121002029	384	0.80	5.3	1.40	0.80	2.0	2.0	He
1121002031	385	0.80	5.3	1.35	0.80	1.7	2.0	He
1121002032	386	0.80	5.3	1.35	0.80	1.7	2.0	He
1121002033	387	0.80	5.3	1.35	0.80	1.8	2.0	He